Prolyl-4-hydroxylase 3 maintains -cell glucose metabolism during fatty acid excess in mice

Nasteska, Daniela; Cuozzo, Federica; Viloria, Katrina; Johnson, Elspeth M; Thakker, Alpesh; Bany Bakar, Rula

Published in:
JCI Insight

DOI:
10.1172/jci.insight.140288

Publication date:
2021

Document Version
Peer reviewed version

JCI insight

Prolyl-4-hydroxylase 3 maintains β-cell glucose metabolism during fatty acid excess in mice

Daniela Nasteska, … , Daniel A. Tennant, David J. Hodson

JCI Insight. 2021. https://doi.org/10.1172/jci.insight.140288.

Research In-Press Preview Endocrinology Metabolism

Graphical abstract

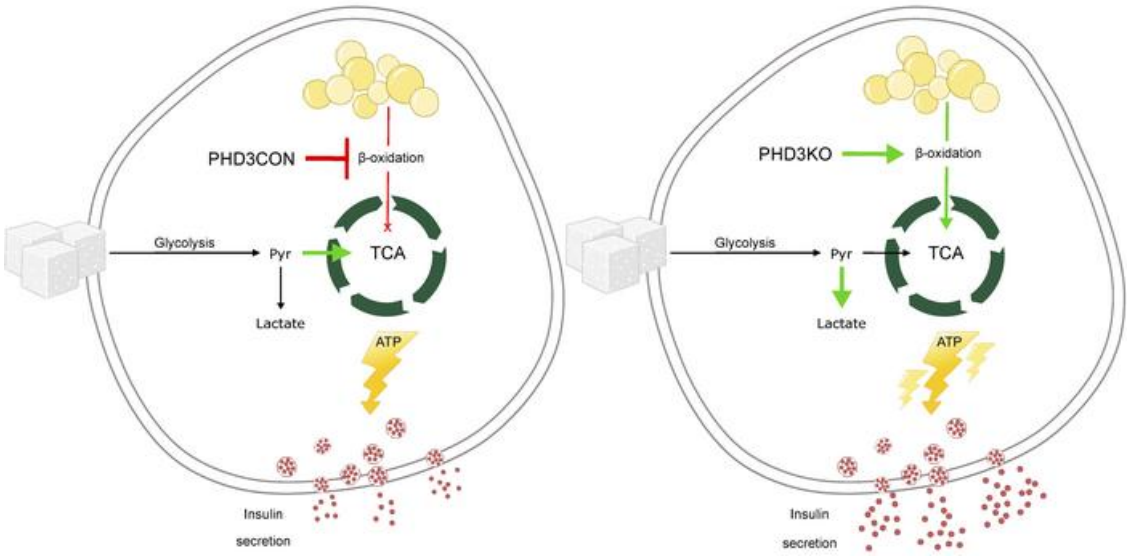

Prolyl-4-hydroxylase 3 maintains β-cell glucose metabolism during fatty acid excess in mice

Daniela Nasteska[1,2,3#], Federica Cuozzo[1,2,3#], Katrina Viloria[1,2,3], Elspeth M. Johnson[4,5], Alpesh Thakker[1,2], Rula Bany Bakar[6], Rebecca L. Westbrook[1,2], Jonathan P. Barlow[7], Monica Hoang[8], Jamie W. Joseph[8], Gareth G. Lavery[1,2], Ildem Akerman[1,2], James Cantley[6,9], Leanne Hodson[4,5], Daniel A. Tennant[1,2]*, David J. Hodson[1,2,3]*

[1] Institute of Metabolism and Systems Research (IMSR), University of Birmingham, Birmingham, UK.
[2] Centre for Endocrinology, Diabetes and Metabolism, Birmingham Health Partners, Birmingham, UK.
[3] Centre of Membrane Proteins and Receptors (COMPARE), University of Birmingham, Birmingham, UK.
[4] Oxford Centre for Diabetes, Endocrinology and Metabolism, University of Oxford, Oxford, UK.
[5] Oxford NIHR Biomedical Research Centre, Churchill Hospital, Oxford, UK.
[6] Department of Physiology, Anatomy and Genetics, University of Oxford, Parks Road, Oxford, UK.
[7] Mitochondrial Profiling Centre, School of Sport, Exercise and Rehabilitation Sciences, University of Birmingham, Birmingham, UK.
[8] School of Pharmacy, University of Waterloo, Kitchener, Ontario, Canada.
[9] Division of Systems Medicine, School of Medicine, University of Dundee, Dundee, UK.

[#]These authors contributed equally

*Correspondence should be addressed to: d.tennant@bham.ac.uk or d.hodson@bham.ac.uk

Institute of Metabolism & Systems Research (IMSR), IBR Tower, College of Medical and Dental Sciences, Birmingham B15 2TT, United Kingdom

Word count (including abstract, references and figure legends): 10,961

Conflict of interest: The authors have declared that no conflict of interest exists.

ABSTRACT

The alpha ketoglutarate-dependent dioxygenase, prolyl-4-hydroxylase 3 (PHD3), is a Hypoxia-Inducible Factor (HIF) target that uses molecular oxygen to hydroxylate peptidyl prolyl residues. While PHD3 has been reported to influence cancer cell metabolism and liver insulin sensitivity, relatively little is known about effects of this highly conserved enzyme in insulin-secreting β-cells *in vivo*. Here, we show that deletion of PHD3 specifically in β-cells (βPHD3KO) is associated with impaired glucose homeostasis in mice fed high fat diet. In the early stages of dietary fat excess, βPHD3KO islets energetically rewire, leading to defects in the management of pyruvate fate and a shift from glycolysis to increased fatty acid oxidation (FAO). However, under more prolonged metabolic stress, this switch to preferential FAO in βPHD3KO islets is associated with impaired glucose-stimulated ATP/ADP rises, Ca^{2+} fluxes and insulin secretion. Thus, PHD3 might be a pivotal component of the β-cell glucose metabolism machinery in mice by suppressing the use of fatty acids as a primary fuel source during the early phases of metabolic stress.

INTRODUCTION

The prolyl-hydroxylase domain proteins (PHD1-3) encoded for by the Egl nine homolog genes are alpha ketoglutarate-dependent dioxygenases, which regulate cell function by catalyzing hydroxylation of peptidyl prolyl residues within various substrates using molecular oxygen (1-4). There are three well-described mammalian isozymes: PHD1, PHD2 and PHD3, which were originally described as hydroxylating the alpha subunit of the transcription factor Hypoxia-Inducible Factor (HIF) under normoxia (4), thus targeting it for polyubiquitylation and proteasomal degradation. When oxygen concentration becomes limited, PHD activity decreases and HIF is stabilized, leading to dimerization with the beta subunit and transcriptional regulation of target genes regulating the cellular response to hypoxia (5). While PHDs are generally regarded to be master HIF regulators, it is becoming increasingly apparent that they target a range of other substrates influencing cell function (6-9).

PHD3 is unusual amongst the PHDs: it is transcriptionally regulated by HIF1 during hypoxia (10), although it does not always act to destabilize HIF1 (11, 12). A number of roles for PHD3 have been described under conditions of stress or hypoxia, including: macrophage influx and neutrophil survival (13, 14), apoptosis in various cancer models (8, 15, 16), and tumor cell survival (9) (reviewed in (17)). Due to the dependence of PHD3 on alpha-ketoglutarate and oxygen for its activity (18), many of these actions are likely to be mediated through alterations in cell metabolism (19). Indeed, PHD3 increases glucose uptake in cancer cells through interactions with pyruvate kinase M2 (8, 20). In tumors exhibiting mutations in succinate dehydrogenase, fumarate hydratase and isocitrate dehydrogenase 1 and 2 (21-23), PHD3 activity is altered by aberrantly high cytosolic concentrations of succinate, fumarate and 2-hydroxyglutarate (2-HG), suggesting that inactivation of this enzyme might be involved in the cellular transformation process. PHD3 has more recently been shown to hydroxylate and activate acetyl-CoA carboxylase 2 (ACC2), defined as the fatty acid oxidation gatekeeper, thus decreasing fatty acid breakdown and restraining myeloid cell proliferation during nutrient

abundance (24). Together, these studies place PHD3 as a central player in the regulation of glucose and fatty acid utilization with clear implications for metabolic disease risk.

Along these lines, PHD3 has been reported to influence insulin sensitivity in the liver (25, 26), as well as maintain glucose-stimulated insulin secretion in a rat β-cell line (27). However, little is known about how PHD3 might contribute to glucose homeostasis and diabetes risk through effects directly in primary pancreatic β-cells. To ensure the appropriate release of insulin, β-cells have become well-adapted as glucose sensors. Thus, glucose enters the β-cell by facilitated diffusion through low affinity glucose transporters (28), before conversion into glucose-6-phosphate by glucokinase and subsequent splitting into pyruvate (29). The pyruvate then undergoes oxidative metabolism in the mitochondrial matrix through the tricarboxylic acid (TCA) cycle, driving increases in ATP/ADP ratio and leading to closure of ATP-sensitive K^+ channels (30). This cascade triggers membrane depolarization, opening of voltage-dependent Ca^{2+} channels, influx of Ca^{2+}, and Ca^{2+}-dependent exocytosis of insulin vesicles through interactions with the SNARE machinery (30). Together with repression of hexokinase, monocarboxylic acid transporter 1 and lactate dehydrogenase A (31, 32), stimulus-secretion coupling prevents the inappropriate release of insulin in response to low glucose, amino acids or lactate.

Given its reported roles in dictating fuel preference, we hypothesized that PHD3 might function as a pivotal component of the β-cell glucose-sensing machinery by suppressing the use of fatty acids as an energy source (27). To further investigate PHD3-regulated β-cell function in depth, we subjected a model of β-cell-specific *Egln3*/PHD3 deletion to extensive *in vivo* and *in vitro* characterization, including detailed stable isotope-resolved metabolic tracing. Here, we show that loss of PHD3 causes metabolic remodeling in the early stages of metabolic stress by shifting β-cell fuel source from glucose to fatty acids. However, as metabolic stress becomes more prolonged, this energetic rewiring impairs glucose-dependent ATP/ADP ratios, Ca^{2+} fluxes and insulin secretion.

As such, these studies build upon previous findings on PHD1-3 in islets and β-cells (27), and show that PHD3 likely constitutes a fundamental mechanism to restrain fatty acid utilization and maintain glucose-sensing in β-cells during early stages of metabolic stress.

RESULTS

Confirmation of β-cell-specific PHD3 knockout

We first generated a model of β-cell PHD3 knockout (βPHD3KO) by crossing the *Ins1Cre* deleter strain (33) with animals harboring flox'd alleles for *Egln3* (34), which encodes PHD3. Given recently reported issues with allele-silencing in some *Ins1Cre* colonies (35), we quantified recombination efficiency of our line using *R26-LSL-hM4Di/mCitrine* animals harboring an mCitrine reporter. Immunostaining of *Ins1Cre*$^{+/-}$;*h4MDi*$^{fl/-}$ islets showed *Ins1Cre*-mediated recombination of the flox'd allele in almost all insulin-immunopositive cells (98.3% ± 1.8 %, mean ± SD) (Figure 1A and B), similar to that reported previously by us and others (33, 36, 37). As expected from this, gene expression analyses showed a 2-fold reduction in *Egln3* expression (Figure 1C), the remainder most likely reflecting the relatively higher levels of *Egln3* detected in α-cells, as shown by RNA-seq (38, 39). Loss of *Egln3* in βPHD3KO islets was not associated with compensatory changes in the other Egln paralogs, *Egln1* and *Egln2* (Figure 1D and E). Immunohistochemical analyses showed that, while PHD3 expression was present throughout βPHD3CON islets, it was completely absent from β-cells in βPHD3KO mice (Figure 1F). While *Egln3* is expressed at low abundance in sorted β-cells (38, 39), this is likely to be a result of profound re-oxygenation following dissociation, thus suppressing *Egln3* expression (40). Together, these data show that PHD3 is expressed in β-cells and can be conditionally deleted from this compartment in βPHD3KO animals, thus confirming the validity of the model.

PHD3 does not contribute to glucose homeostasis under standard diet

After confirming *Egln3*/PHD3 deletion, we set out to understand the metabolic phenotype of βPHD3KO mice. βPHD3KO mice presented with normal growth curves from 8-18 weeks of age compared to βPHD3CON littermates, with no apparent differences in male and female cohorts (Figure 2A and B). Intraperitoneal glucose tolerance testing in the same animals showed no abnormalities in glycemia (Figure 2C and D), which was unchanged up until the age of 20 weeks (Figure 2E and F). Likewise, oral glucose tolerance, largely determined by

incretin release from the intestine (41), was similar in βPHD3CON and βPHD3KO mice (Figure 2G and H). As expected from the growth rates and glucose tolerance, both male and female βPHD3KO mice displayed similar insulin sensitivity to their βPHD3CON littermates (Figure 2I and J). Finally, no differences in islet size distribution (Figure 2K) and β-cell mass (Figure 2L and M) were detected in βPHD3KO versus βPHD3CON mice.

PHD3 does not influence β-cell function *in vitro* under standard diet

Isolation of islets for more detailed *in vitro* workup revealed normal expression of the β-cell transcription factors *Pdx1*, *Mafa* and *Nkx6.1* in βPHD3KO islets, suggesting that βcell differentiation is unaffected by loss of PHD3 (Figure 3A). Further suggestive of mature β-cell function, live imaging approaches revealed normal glucose-stimulated Ca^{2+} fluxes (Figure 3B and C) and ATP/ADP ratios (Figure 3D and E) in βPHD3KO islets. Suggesting the presence of intact GLP1R signaling, an important amplifying input for insulin secretion, cAMP responses to the incretin-mimetic Exendin-4 (Figure 3F and G), as well as *Glp1r* expression (Figure 3H) were similar in βPHD3CON and βPHD3KO islets. In line with the Ca^{2+}, ATP/ADP and cAMP analyses, both glucose- and Exendin-4-potentiated insulin secretion were similar in islets isolated from male and female βPHD3CON and βPHD3KO animals (Figure 3I and J).

Loss of PHD3 improves insulin secretion at the onset of metabolic stress

We next examined whether PHD3 might play a more important role in regulating insulin release during metabolic stress. Therefore, male animals were placed on high fat diet (HFD) to induce obesity and metabolic stress (42).

Following 4 weeks HFD, *Egln3* was moderately upregulated in βPHD3CON islets (Figure 4A). However, *Egln3* levels remained suppressed in 4 weeks HFD βPHD3KO islets (Figure 4A). Glucose tolerance testing revealed significantly impaired glucose homeostasis in βPHD3KO mice at 4 weeks but not at 72 hrs HFD (Figure 4B and C), despite similar body weight gain compared to βPHD3CON littermates (Figure 4D). The 72 hour timepoint was used to differentiate effects of early and prolonged fatty acid incorporation/utilization. As expected,

fasting blood glucose levels were elevated in βPHD3CON mice following 4 weeks HFD (Figure 4C). There was no effect of *Cre* or flox'd alleles *per se* on metabolic phenotype following 4 weeks HFD, with *Ins1*$^{wt/wt}$*;Egln3*$^{fl/fl}$, *Ins1Cre*$^{+/-}$*;Egln3*$^{wt/wt}$ and *Ins1*$^{wt/wt}$*;Egln3*$^{wt/wt}$ controls being indistinguishable (Figure 4E). IPGTT at 4 weeks HFD showed no difference in the serum insulin levels between the βPHD3CON and βPHD3KO under fasting and glucose-stimulated conditions (Figure 4F). However, βPHD3KO mice mounted earlier and larger magnitude insulin secretory responses to glucose bolus, as shown by the stimulation index (Figure 4G). Islets isolated from the same animals secreted significantly more insulin in glucose-stimulated and Ex4-potentiated states (Figure 4H), while insulin content was similar to βPHD3CON littermates (Figure 4I). Finally, 4 weeks HFD had no effect on glucose tolerance during OGTT (Figure 4J), body composition (Figure 4K) and insulin sensitivity (Figure 4L) in βPHD3KO mice vs βPHD3CON littermates.

Thus, βPHD3KO mice are glucose-intolerant on HFD, show improved insulin secretion and are able to release a greater fraction of their insulin granules (i.e. are more sensitized to exocytosis). These data raise the possibility that nutrient-sensing and utilization might be altered in βPHD3KO islets.

PHD3 maintains glycolysis and pyruvate management in β-cells

Given the reported roles of PHD3 in glycolysis, we wondered whether the changes in β-cell function observed during the early phases of high fat feeding in βPHD3KO mice might be associated with changes in glucose metabolism. We first looked at glycolytic fluxes using ^{14}C glucose. While glucose oxidation was not altered at low or high glucose in islets from 4 weeks HFD βPHD3KO mice (Figure 5A), there was a small but significant decrease in ^{14}C content in the aqueous phase, indicating a net reduction in tricarboxylic acid (TCA) cycle/other metabolites derived from glycolysis (Figure 5B). Notably, a 2-fold reduction in incorporation of glucose into the lipid pool (i.e. glucose-driven lipogenesis) was also detected in 4 weeks HFD

βPHD3KO islets (Figure 5C), suggestive of decreased oxidative pyruvate entry into the TCA cycle and lipogenic acetyl-CoA (43).

To gain a higher resolution analysis of glucose fate, stable isotope-resolved tracing was performed in βPHD3KO islets using $^{13}C_6$-[U]-glucose. The schematic in Figure 5D depicts the fate of ^{13}C from $^{13}C_6$-[U]-glucose in βPHD3KO islets, as assessed by gas chromatography-mass spectrometry (GC-MS). Analysis of mass isotopomer distribution showed no differences in glucose incorporation into aspartate, glutamate, malate, fumarate or citrate in either standard chow or 4 weeks HFD βPHD3CON and βPHD3KO islets (Figure 5E-I). Thus, while the contribution of glucose to aqueous cellular metabolite pools is clearly reduced in 4 weeks HFD βPHD3KO islets (Figure 5B), there is no net change in the incorporation of glucose into each metabolite i.e. the TCA cycle proceeds normally despite lowered glucose fluxes. Islets from animals fed standard chow showed m+2 lactate accumulation (Figure 5J), which is consistent with lactate normally produced as a result of oxidative metabolism of glucose-derived pyruvate. However, during HFD there was a pronounced switch to reduction of pyruvate to lactate (indicated by the m+3 isotopomer) in both genotypes (Figure 5J).

Further analysis of steady-state lactate levels showed a significant increase in lactate production in islets from HFD-fed βPHD3KO versus βPHD3CON mice (Figure 5K). Together with the m+2 → m+3 switch, this finding confirms initial measures with ^{14}C glucose indicating reduced fueling of the TCA cycle by glycolysis (Figure 5B). Furthermore, the tracing data suggest that 4 weeks HFD βPHD3KO islets increase the reduction of pyruvate → lactate to support continued glycolysis through regeneration of the cytosolic NAD^+ pool. While expression of the “disallowed gene” *Ldha* (31, 32) tended to be increased, this was variable and not significantly different between βPHD3CON and βPHD3KO islets. (Figure 5L).

Together, these data suggest that metabolic stress induces defects in the management of pyruvate fate in βPHD3KO islets, implying that insulin secretion *in vitro* must be maintained and even amplified through mechanisms other than glycolysis.

PHD3 suppresses fatty acid use under metabolic stress

We hypothesized that βPHD3KO islets might switch to an alternative energy source to sustain their function, namely beta oxidation of fatty acids, which are present in excess during HFD. Moreover, in cancer cells PHD3 has been shown to increase activity of ACC2, which converts acetyl-CoA → malonyl-CoA, the latter suppressing carnitine palmitoyltransferase I (CPT1), the rate-limiting step in fatty acid oxidation (24, 44). Indicating a profound change in β-cell nutrient preference, supplementation of culture medium with the fatty acid palmitate for 48-72 hrs augmented glucose-stimulated and Exendin4-potentiated insulin secretion in 4 weeks HFD βPHD3KO islets (Figure 6A). By contrast, 4 weeks HFD βPHD3CON islets showed no increase in glucose-stimulated insulin release following culture with palmitate (Figure 6B), confirming that the fatty acid was unlikely to induce lipotoxicity at the concentration and timing used here. Interestingly, 48-72 hrs incubation with palmitate increased Exendin4-potentiated insulin secretion in 4 weeks HFD βPHD3CON islets (Figure 6B).

Providing evidence for increased CPT1 activity in 4 weeks HFD βPHD3KO islets, the CPT1a inhibitor etomoxir was able to augment ATP/ADP responses to glucose in 4 weeks HFD βPHD3KO relative to βPHD3CON islets (Figure 6C), although mRNA levels of *Cpt1a* were similar (Figure 6D). In line with this finding, culture with low palmitate concentration decreased glucose-stimulated Ca^{2+} fluxes in 4 weeks HFD βPHD3KO but not in βPHD3CON islets (Figure 6E and F), presumably due to increased flux of fatty acid-derived acetyl-CoA into the TCA cycle. While glucose-driven Ca^{2+} fluxes were apparently normal in 4 weeks HFD βPHD3KO islets, this was likely due to increased sensitivity of voltage-dependent Ca^{2+} channel to membrane depolarization, since responses to KCl were significantly elevated (Figure 6G and H).

To gain a higher resolution view of fatty acid fate, we incubated 4 weeks HFD βPHD3CON and βPHD3KO islets with D31-palmitate, before measurement of intracellular D31-palmitate concentration and $2H_20$ released from fatty acid oxidation. With this assay, the ratio of $2H_20$

to intracellular D31-palmitate provides a measure of fatty acid oxidation, whilst accounting for any differences between tracer uptake/turnover. Confirming accuracy of the assay, $2H_20$/D31-palmitate values were robustly increased after 16 hrs versus 2 hrs incubation with tracer (Figure 6I).Notably, $2H_20$/D31-palmitate values were significantly higher in 4 weeks HFD βPHD3KO versus βPHD3CON islets at the 16 hrs timepoint (Figure 6I), indicative of higher fatty acid oxidation rates. Uptake of tracer was similar in βPHD3KO versus βPHD3CON islets (Figure 6J).

Taken together, these data strongly suggest that PHD3 loss leads to alterations in fatty acid utilization in islets.

Loss of PHD3 decreases dependency on glucose as a fuel source

We wondered whether increased fatty acid utilization in 4 weeks HFD βPHD3KO islets was associated with a decreased dependency on glucose as a primary fuel source. Confirming a switch away from glycolysis, glucose-stimulated ATP/ADP ratios were markedly decreased in 4 weeks HFD βPHD3KO islets (Figure 6K and L), despite the apparent increases in insulin secretion (Figure 6A). Moreover, steady-state pyruvate levels were decreased in 4 weeks HFD βPHD3KO islets (Figure 6M). Lastly, glucose-stimulated insulin secretion (GSIS) was impaired in SC βPHD3KO islets that were starved of glucose (3 mM) for 3 hrs prior to challenge (Figure 6N), presumably due to dysregulated use of alternative fuel sources, which then inhibit critical metabolic hubs in central carbon metabolism, such as pyruvate dehydrogenase. These data further confirm the presence of defective pyruvate handling and suggest that βPHD3KO islets alter pyruvate production and/or increase pyruvate → lactate conversion to maintain redox balance during HFD.

Thus, following 4 weeks HFD, βPHD3KO islets become less reliant on glycolysis to fuel ATP/ADP production, are able to sustain oxidative phosphorylation through fatty acid use, and secrete more insulin when both glucose and fatty acids are present.

Regulated gene expression of ACC1 and ACC2 in β-cells

Previous studies have shown that PHD3 maintains glucose metabolism by hydroxylating and activating ACC2 (encoded by *Acacb)*, which inhibits CPT1 through generation of mitochondrial malonyl-CoA, thus suppressing use of fatty acids via beta oxidation (45, 46). However, β-cells are thought to predominantly express ACC1 (encoded by *Acaca)* (45, 46), which supplies cytosolic malonyl-CoA to fatty acid synthase for *de novo* lipid biosynthesis rather than for beta oxidation (43). Therefore, we sought to determine whether it was possible for PHD3 to act via ACC2 in pancreatic β-cells. We re-examined the expression of *ACACB* in pancreatic β-cells in multiple well-powered bulk islet and purified β-cell gene expression datasets (38, 47, 48). *ACACB* mRNA was found to be present in β-cells, albeit at much lower levels than *ACACA* mRNA (Supplementary figure 1A). Our data suggests that the presence of *ACACB* mRNA in β-cells is not artefactual: first, the mRNA levels of *ACACB* are comparable to the β-cell transcription factor *HNF1A,* suggesting ample gene expression levels compatible with function (Supplementary figure 1A). Second, the *ACACB* gene promoter is bound by islet and β-cell specific transcription factors, suggesting that *ACACB* is a bona fide β-cell gene under the regulation of cell-specific transcription factors (Supplementary figure 1B). Our findings thus suggest that, as long as protein translation occurs, PHD3 could maintain glucose metabolism in pancreatic β-cells via hydroxylation of ACC2. We next examined if *ACACB* gene expression is under the regulation of PHD3 protein. Gene expression levels of *Acaca* and *Acacb* were similar in 4 weeks HFD βPHD3KO and βPHD3KO islets (Figure 7A and B), suggesting that *Acacb* mRNA levels are not regulated by PHD3 activity.

Thus, *ACACB* is present in β-cells, contains promoter regions regulated by β-cell-specific transcription factors, but does not depend upon PHD3 for expression. These data are consistent with a scenario whereby PHD3 hydroxylates ACC2 without influencing mRNA expression.

PHD3 protects against insulin secretory failure during prolonged metabolic stress

Lastly, we sought to understand the phenotype of βPHD3KO mice when faced with continued fatty acid/nutrient abundance. Glucose intolerance was still present in βPHD3KO mice following 8 weeks on HFD (Figure 7C), although less severe than at 4 weeks HFD, suggesting that metabolic rewiring might in fact be protective against prolonged exposure to excess fatty acids *in vivo*. As was the case at 4 weeks HFD, βPHD3KO mice showed similar insulin sensitivity to βPHD3CON after 8 weeks HFD (Figure 7D). In contrast to the IPGTT data, oral glucose tolerance was preserved at this time point in βPHD3KO mice, suggesting an intact incretin action (Figure 7E). Furthermore, body composition of 8 weeks HFD βPHD3KO mice was similar to βPHDCON (Figure 7F). By this point, however, impaired glucose-stimulated insulin secretion (Figure 7G) was apparent in isolated βPHD3KO islets. This secretory deficit could be rescued by application of Exendin4 to sensitize insulin granules to exocytosis (Figure 7G and H), as expected from the OGTT results. In addition, the amplitude of glucose-stimulated Ca^{2+} rises was significantly reduced in 8 weeks HFD βPHD3KO compared to βPHD3CON islets (Figure 7I and J).

Suggesting that profound defects in voltage-dependent Ca^{2+} channels might also be present, responses to the generic depolarizing stimulus KCl were markedly blunted in the same islets (Figure 7I and J). While apoptosis was increased in 8 weeks HFD βPHD3KO islets (Figure 7K and L), this did not reflect a (detectable) lipotoxic ER stress response, since *Ddit3, Hspa5* and *Xbp1* (Figure 7M) expression remained unchanged. Moreover, PCNA staining (Figure 7N and O) and α-cell/β-cell ratio (Figure 7P and Q) were similar in 8 weeks HFD βPHD3CON and βPHD3KO islets, suggesting that β-cells were unlikely to be less/more proliferative or adopting α-cell features (or vice versa). Nonetheless, a profound 2-fold increase in β-cell mass was observed in 8 weeks HFD βPHD3KO mice (Figure 7R and S), with a significant increase in the proportion of larger islets (Figure 7T), implying that either: 1) apoptosis was restricted to smaller/medium islets; or 2) changes in apoptosis/proliferation rate had not yet been able to counter previous β-cell mass expansion.

Loss of PHD3 is not associated with changes in HIF stabilization

Previous studies have shown that PHD3 is highly regulated at the transcriptomic level by hypoxia (10), and in line with this, we also found that *Egln3* levels in WT islets were increased under hypoxic (1% O_2) conditions (Supplementary figure 2A). To account for HIF-dependent effects on β-cell phenotype in SC βPHD3KO animals, a number of canonical HIF1α-target genes were assessed. Notably, levels of *Bnip3*, *Car9* and *Gls* were similar between normoxic (21% O_2) SC βPHD3CON and βPHD3KO islets (Supplementary figure 2B-D). Further suggesting the presence of intact HIF signaling, *Bnip3* and *Car9* were upregulated to similar levels in hypoxic (1% O_2) SC βPHD3CON and βPHD3KO islets, while *Gls* did not reliably increase (Supplementary figure 2B-D). Glucose and KCl-stimulated Ca^{2+} fluxes, shown to be sensitive to HIF stabilization (49), were similar in βPHD3CON and βPHD3KO islets exposed to hypoxia (Supplementary figure 2E-H).

Suggesting that stabilization of HIF1α and HIF2α was unlikely to be a major feature in 4 weeks HFD βPHD3KO islets, *Bnip3*, *Car9* and *Gls* levels were similar to βPHD3CON (Supplementary figure 2I-K). Furthermore, at 8 weeks HFD the HIF2α target *Ccnd1* remained similar in βPHD3CON and βPHD3KO islets, while gene *Dll4* was downregulated (Supplementary figure 2L and M).

DISCUSSION

In the present study, we show that the alpha-ketoglutarate-dependent PHD3 maintains β-cell glucose sensing under states of metabolic stress associated with fatty acid abundance. Our data suggest that PHD3 is required for ensuring that acetyl-CoA derived from glycolysis preferentially feeds the TCA cycle, linking blood glucose levels with ATP/ADP generation, β-cell electrical activity and insulin secretion. Loss of PHD3 leads to metabolic remodeling under HFD, resulting in decreased glycolytic fluxes, an increase in lactate accumulation and utilization of fatty acids as an energy source. Thus, PHD3 appears to be a critical component of the β-cell metabolic machinery required for glucose sensing during episodes of nutritional overload (Figure 8).

Previous studies have shown that the PHD1-3 inhibitor ethyl-3,4-dihydroxybenzoate (EDHB) exerts bimodal effects on islets: low concentrations increase GSIS, while high doses impair GSIS (27). Suggesting that these changes are mediated primarily by PHD3, siRNAs against PHD1 and PHD2 were without effect on GSIS in INS1-832/13 clonal rat β-cells, whereas PHD3 siRNA markedly blunted release of the hormone (27). Using a conditional knockout model, our studies extend these findings to primary islets and provide further mechanistic evidence for a critical role of PHD3 in β-cell metabolism and function. A key difference between the studies is that PHD3 loss only impairs GSIS in islets exposed to metabolic stress (HFD), whereas effects were apparent in INS1-832/13 under normal culture conditions. The most likely explanation for this finding is the different metabolic dependencies of primary islets versus proliferative, immortalized β-cells.

How does PHD3 maintain glucose metabolism in β-cells? Previous studies in cancer cells and skeletal muscle have shown that PHD3 hydroxylates and activates ACC2, suppressing beta oxidation (24). While β-cells are thought to predominantly express ACC1, the levels of *ACACB*, which encodes ACC2, were found to be similar to the β-cell transcription factor HNF1A, albeit lower than those of *ACACA*. We thus propose that loss of PHD3 might

plausibly lead to suppression of ACC2 activity, which becomes apparent during HFD when its substrate is present in abundance. Alternatively, PHD3 might hydroxylate and activate ACC1, leading to regulation of CPT1 by malonyl-CoA when fatty acids are supplied in excess, as suggested by glucose oxidation experiments. In both cases, identifying the PHD3 hydroxylation sites involved will be critical. However, assigning hydroxylation targets using mass spectrometry is currently controversial: mis-alignment of hydroxylation is frequently associated with the presence of residues in the tryptic fragment that can be artefactually oxidized (44, 50). Thus, studies using animals lacking PHD3 and ACC1/ACC2 in β-cells, or alternatively the use of (relatively) specific inhibitors, would be required to definitively link the carboxylase with the phenotype here.

As normal chow contains a low proportion of calories from fat, metabolic stress was needed to reveal the full *in vitro* and *in vivo* phenotype associated with PHD3 loss. These data also support an effect of PHD3 on ACC1/2 and CPT1, since without acyl-CoA derived from exogenous fatty acids, glucose would still constitute the primary fuel source and regulator of insulin release. The lack of phenotype under normal diet is unlikely to reflect the age of the animals, since even at 20 weeks of age, glucose intolerance was still not present in βPHD3KO mice. Of interest, the severity of the βPHD3KO *in viv*o phenotype was milder at 8 weeks versus 4 weeks HFD feeding, despite the presence of impaired glucose-dependent β-cell function by this timepoint. These observations suggest that, by 8 weeks HFD, compensatory protective mechanisms may become upregulated as a consequence of the metabolic re-wiring in β-cells. It will be necessary in the future to investigate the mechanistic/phenotypic changes occurring during even longer duration HFD feeding (e.g. 12-20 wks). It will also be interesting to understand how PHD3 activity changes in other models of metabolic stress, such as *db/db* and *ob/ob* mice.

Suggesting that the phenotype associated with PHD3 loss was not due to changes in HIF signaling, no differences in the gene expression of HIF1 targets could be detected in βPHD3KO versus βPHD3CON islets. Indeed, PHD2 is the major hydroxylase that regulates

HIF1α stability (11, 12), with no changes in activity of the transcription factor following PHD3 loss (11, 12, 51). Thus, it is perhaps unsurprising that there is a lack of HIF1 transcriptional signature in βPHD3KO islets, in agreement with previous studies in other tissues (51, 52). In addition, glucose-stimulated Ca^{2+} fluxes, a sensitive readout of changes in oxygen-dependent regulation (49), were unaffected during hypoxia in βPHD3KO islets. While there was a trend toward increased *Ldha* expression in HFD βPHD3KO islets, this was just a fraction of that previously reported in hypoxic rodent islets (53). Nonetheless, we cannot completely exclude HIF-dependent effects, and as such, studies should either be repeated on a HIF1- and HIF2-null background (i.e. a quadruple transgenic) or using (moderately) specific chemical inhibitors.

We acknowledge a number of limitations with the present studies. Firstly, work-up was limited to rodents and it will be important to confirm whether results translate to human islets or not. While our attempts at silencing PHD3 using *EGLN3* shRNA were unsuccessful, studies using (relatively) specific PHD3 inhibitors are warranted. Secondly, interactions between PHD3 and ACC2 are inferred from our metabolic work up and known biochemistry. Identifying hydroxylation sites and creating corresponding ACC1/2 mutants is needed, but current mass spectrometry analysis is challenging due to the assignment of false positives, as mentioned above. Thirdly, we focused our studies on 4 and 8 weeks HFD and it is unclear whether the switch toward increased fatty acid utilization might be maladaptive or protective in βPHD3KO mice during longer periods of HFD feeding. Fourthly, HFD studies were restricted to male animals and further studies should be extended to female animals. While sex differences in phenotype were not observed under standard diet, we cannot exclude a sexually dimorphic effect of HFD. In summary, PHD3 possesses a conserved role in gating nutrient preference toward glucose and glycolysis during both cell transformation (24) and metabolic stress (as shown here). It will be interesting to now study whether similar effects of PHD3 are present in other cell types involved in glucose-sensing (for example, pancreatic alpha cells, hypothalamic neurons).

METHODS

Experimental design

No data were excluded unless the cells displayed a non-physiological state (i.e. impaired viability). All individual data points are reported. The measurement unit is animal or batch of islets, with experiments replicated independently. Animals and islets were randomly allocated to treatment groups to ensure that all states were represented in the different experiment arms.

Mouse models

β-cell-specific PHD3 (βPHD3KO) knockout mice were generated using the Cre-LoxP system. *Ins1Cre* mice (JAX stock no. 026801), with Cre-recombinase knocked into the *Ins1* gene locus, were crossbred to mice carrying flox'd alleles for PHD3 (*Egln3*$^{fl/fl}$) (34). Adult βPHD3KO animals (*Ins1Cre*$^{+/-}$*;Egln3*$^{fl/fl}$) and their controls (βPHD3CON) (*Ins1*$^{wt/wt}$*;Egln3*$^{fl/fl}$, *Ins1Cre*$^{+/-}$*;Egln3*$^{wt/wt}$ and *Ins1*$^{wt/wt}$*;Egln3*$^{wt/wt}$) were used from 8-20 weeks of age under both standard diet and high fat diet conditions. No extra-pancreatic recombination has been observed in *Ins1Cre* mice and possession of a *Cre* allele is not associated with any changes in glucose homeostasis in our hands (33, 36). Recombination efficiency of the *Ins1Cre* allele was checked using a *R26-LSL-hM4Di/mCitrine* (JAX stock no. 026219) DREADD reporter strain. Animals were maintained on a C57BL/6J background and backcrossed for at least 6 generations following re-derivation into the animal facility. Lines were regularly refreshed by crossing to bought-in C57BL/6J (Charles River). Wild type male CD1 mice aged 8-12 weeks (Charles River) were used for confirmation of gene expression under hypoxic (1% O_2) conditions. βPHD3CON and βPHD3KO mice were fed standard chow (SC) and/or high fat diet containing 60% fat (HFD), (Research Diets, cat.no.D12492), with body weight checked weekly until 18-20 weeks of age. Animals were maintained in a specific pathogen-free facility, with free access to food and water.

Intraperitoneal and oral glucose tolerance testing

Mice were fasted for 4-6 hrs, before intraperitoneal injection of glucose. Animals on SC received 2 g/kg body weight glucose, whereas those on HFD received a lower dose of 1 g/kg body weight. In our hands, this allows measurement of blood glucose concentration without the need to dilute samples and decreases adverse reactions associated with profound hyperglycemia. Blood samples for glucose measurement were taken from the tail vein at 0, 15, 30, 60, 90 and 120 min post-challenge. Glucose was measured using a Contour XT glucometer (Bayer, Germany). For mice on SC, intraperitoneal glucose tolerance testing (IPGTT) was performed every 2-4 weeks, between 8-20 weeks of age. HFD-fed mice underwent IPGTT following 72 hrs, 4 and 8 weeks of HFD. Oral glucose tolerance testing (OGTT) was performed as for IPGTT, except that glucose was delivered using an oral gavage tube (2 g/kg and 1 g/kg body weight in SC-fed and HFD-fed mice, respectively) .

Serum insulin

Blood samples were collected following intraperitoneal glucose injection (1 g/kg body weight). Serum was separated by centrifugation (2500 rpm/10 min/4°C), before assaying using a HTRF Mouse Serum Insulin Assay kit assay (Cisbio, France). Due to NC3R limits on blood sample volumes, insulin was only measured at 0, 15 and 30 min post-glucose injection.

Insulin tolerance test (ITT)

Mice fasted for 4-6 hrs (SC and 4 weeks HFD cohorts) or overnight (8 weeks HFD cohort) received 0.75 U/kg body weight insulin (Humulin S, 100 U/ml, Lilly, UK) given by intraperitoneal injection. Blood glucose was measured at 0, 15, 30, 60, 90 and 120 min post-insulin injection.

Body composition measurement

Male βPHD3CON and βPHD3KO mice fed HFD for 4 and 8 weeks were weighed and sacrificed by cervical dislocation. The followed tissues were harvested and weighed immediately post-mortem: visceral fat (epididymal fat pads), subcutaneous fat, brown adipose

tissue, liver and muscle (quadriceps femoris). Tissue contribution to body composition was expressed as % body weight.

Islet isolation

Islets were isolated following bile duct injection with NB8 1 mg/ml collagenase (Serva) and Histopaque/Ficoll gradient separation (Sigma-Aldrich). Islets were cultured in RPMI medium containing 10% FCS, 100 units/mL penicillin, and 100 µg/mL streptomycin (Sigma-Aldrich) at 5% CO_2, 37°C. For experiments under hypoxia, islets were incubated in a Don Whitely H35 Hypoxystation, allowing oxygen tension to be finely regulated at either 1% or 21%.

Gene expression

Trizol purification was used for mRNA extraction, while cDNA was synthesized by reverse transcription. Gene expression was detected by real time PCR (qPCR), using PowerUp SYBR Green Master Mix (Thermofisher Scientific) and quantification was based on the $2^{-\Delta\Delta Ct}$ method, expressed as fold-change in gene expression. The sequence of the forward and reverse primers used in the study can be found in Supplementary Table 1.

Immunohistochemistry

Pancreata were isolated, fixed in 10% formalin and embedded in paraffin. Paraffin slides were deparaffinized and rehydrated, before antigen retrieval using citrate buffer. Sections stained for PHD3 were incubated overnight at 4°C with guinea pig anti-insulin 1:100 (Abcam, ab7842) and rabbit anti-PHD3 1:100 (Novus Bio, NB100-139), followed by washing and 2h incubation at room temperature with anti-guinea pig Alexa Fluor 568 1:300 (ThermoFisher Scientific, A-11075) and anti-rabbit Alexa Fluor 488 1:1000 (ThermoFisher Scientific, A-21206). PCNA staining was carried out using rabbit anti-insulin 1:500 (Cell Signaling, 3014S) and mouse anti-PCNA 1:500 (Cell Signaling, 2586) as primary antibodies. Secondary antibodies used were anti-rabbit Alexa Fluor 568 1:500 (ThermoFisher Scientific, A-10042) and anti-mouse Alexa

Fluor 488 (ThermoFisher Scientific; A11001). VECTASHIELD HardSet mounting medium with DAPI was used to mount coverslips on the sections.

Images were taken using a Zeiss LSM780 meta-confocal microscope equipped with highly-sensitive GaAsP PMT detectors. Excitation was delivered at λ = 405 nm, λ = 488 nm and λ = 561 nm for DAPI, Alexa Fluor 488 and Alexa Fluor 568, respectively. For PHD3 staining, the emitted signals were detected at λ = 410-472 nm, λ = 507-596 nm and λ = 561-694 nm, for DAPI, Alexa Fluor 488 and Alexa Fluor 568, respectively. For PCNA staining, emitted signals were detected at λ = 418-507 nm, λ = 507-552 nm and λ = 579-641 nm for DAPI, Alexa Fluor 488 and Alexa Fluor 568, respectively.

TUNEL staining was performed using the DeadEnd Fluorometric TUNEL System (Promega), as previously described (54). The proportion of apoptotic β-cells was calculated as the area of TUNEL+ staining (fluorescein-12-dUTP)/area of insulin+ staining (as above). α-cell/ β-cell ratio was calculated following staining with rabbit antibodies against insulin (as above) and glucagon (primary antibody: mouse anti-glucagon 1:2000; Sigma-Aldrich, G2645) (secondary antibody goat anti-mouse Alexa Fluor 488 1:500; ThermoFisher Scientific, A11001). Images were captured as above. Excitation was delivered at λ = 405 nm, λ = 488 nm and λ = 633 nm for DAPI, fluorescein-12-dUTP/Alexa Fluor 488 and Alexa Fluor 647, respectively. Emitted signals were detected at λ = 428-533 nm, λ = 498-559 nm and λ = 643–735 nm for DAPI, fluorescein-12-dUTP/Alexa Fluor 488 and Alexa Fluor 633, respectively. For β-cell mass analysis, sections were incubated with rabbit anti-insulin 1:500 (Cell Signaling, 3014S) and mouse anti-glucagon 1:2000 (Sigma-Aldrich, G 2654) followed by washing and application of goat anti-rabbit Alexa Fluor 647 1:500 (ThermoFisher Scientific, A-21244) and goat anti-mouse DyLight 488 1:500 (Invitrogen, 35503). Coverslips were mounted using VECTASHIELD HardSet with DAPI and 425 images per section captured using a Zeiss Axio Scan.Z1 automated slide scanner equipped with a 20 x / 0.8 NA objective. β-cell mass (%) was calculated as the area of insulin-positive staining/area of the pancreas. Excitation was delivered at λ = 330-375 nm and λ = 590-650 nm for DAPI and Alexa Fluor 647, respectively.

Emitted signals were detected using an Orca Flash 4.0 at λ = 430-470 nm and λ = 663-738 nm for DAPI and Alexa Fluor 647, respectively.

Insulin secretion *in vitro* and insulin measurement

Ten to fifteen size-matched islets were stimulated with: 3 mM glucose, 16.7 mM glucose and 16.7 mM glucose + 20 nM Exendin-4 in HEPES-bicarbonate buffer (mM: 120 NaCl, 4.8 KCl, 24 $NaHCO_3$, 0.5 Na_2HPO_4, 5 HEPES, 2.5 $CaCl_2$, 1.2 $MgCl_2$; Sigma-Aldrich) supplemented with 0.1% BSA at 37°C. Insulin content was extracted using acid ethanol. Insulin concentration (ng/ml) was measured using a HTRF Insulin Ultra-Sensitive Assay kit (Cisbio, 62IN2PEG). For experiments with exogenous lipids, islets were treated with either 0.75% bovine serum albumin (BSA) control, or 150 µM sodium palmitate dissolved in 0.75% BSA for 48-72 hrs before the secretion assay. This concentration and timing do not induce profound lipotoxicity in our hands, allowing the study of metabolic phenotype in the absence of β-cell failure.

Live imaging

Islets were loaded with the Ca^{2+} indicators Fluo8 (AAT Bioquest, 21083) or Fura2 (AAT Bioquest, 21020), before imaging using a Crest X-Light spinning disk microscope coupled to a Nikon Ti-E base with 10 x 0.4 NA and 20 x 0.8 NA objectives. For Fluo8 imaging, excitation was delivered at and λ = 458–482 nm using a Lumencor Spectra X light engine. Emission was captured at λ = 500-550 nm using a highly-sensitive Photometrics Delta Evolve EM-CCD. For experiments with the ratiometric Ca^{2+} indicator, Fura2, excitation was delivered at λ = 340 nm and λ = 385 nm using Cairn Research Fura LEDs in widefield mode, with emitted signals detected at λ = 470–550 nm.

For ATP/ADP imaging, islets were transduced with the ATP/ADP sensor Perceval (a kind gift from Prof Gary Yellen, Harvard University, Boston, USA) (55) using an adenoviral vector and imaged identically to Fluo8. For FRET-based cAMP imaging, islets were infected with adenovirus harboring Epac2-camps (a kind gift from Prof Dermot Cooper, University of Cambridge, Cambridge, United Kingdom). Excitation was delivered at 430–450 nm, with

emission detected at and λ = 460–500 and and λ = 520–550 nm for Cerulean and Citrine, respectively.

In all cases, HEPES-bicarbonate buffer was used (mM: 120 NaCl, 4.8 KCl, 24 $NaHCO_3$, 0.5 Na_2HPO_4, 5 HEPES, 2.5 $CaCl_2$, 1.2 $MgCl_2$, and 3–17 D-glucose), with glucose and drugs (Exendin-4, Sigma-Aldrich E144-.1MG and etomoxir, Sigma-Aldrich E1905-5MG) being added at the indicated concentrations and timepoints. Fura2 and Epac2-camps traces were normalized as the ratio of 340/385 or Cerulean/Citrine, respectively. Data were presented as raw or F/F_{min} where F = fluorescence at any timepoint and F_{min} = minimum fluorescence, or R/R_0 where R = fluorescence at any timepoint and R_0 = fluorescence at 0 mins.

Glucose oxidation assays and metabolic tracing

^{14}C glucose oxidation and lipid incorporation: batches of 40 islets were used for quantification of ^{14}C glucose (Perkin-Elmer) oxidation and incorporation into lipids by scintillation spectrometry, as previously described (43).

Gas chromatography–mass spectrometry (GC-MS)-based $^{13}C_6$ mass isotopomer distribution: To ensure steady state, 50-100 islets were cultured with 10 mM $^{13}C_6$-[U]-glucose (Sigma-Aldrich, 389374) for 24 hrs (56), before extraction of metabolites using sequentially pre-chilled HPLC-grade methanol, HPLC-grade distilled H_2O containing 1 µg/mL D6-glutaric acid and HPLC-grade chloroform at -20 ˚C (all from Sigma-Aldrich). Polar fractions were separated by centrifugation, vacuum dried and solubilized in 2% methoxyamine hydrochloric acid in pyridine (Fisher Scientific). Samples were derivatized using N-tertbutyldimethylsilyl-N-methyltrifluoroacetamide (MTBSTFA) with 1% (w/v) tertbutyldimethyl-chlorosilane (TBDMCS) (both from Sigma-Aldrich), before analysis on an Agilent 7890B gas chromatograph mass spectrometer, equipped with a medium polar range polydimethylsiloxane GC column (DB35-MS). Mass isotopomer distributions (MIDs) were determined based upon spectra corrected for natural isotope abundance. Data were analyzed using MetaboliteDetector software (57).

D31-palmitate incorporation and oxidation assays

For D31-palmitate tracing, 140 islets per genotype were cultured at 5% CO_2, 37°C, in a solution of 150 µM D31-palmitic acid (98%; Cambridge Isotope Laboratories, DLM-215-1), dissolved in RPMI supplemented with 10% FBS, 100 units/mL penicillin, 100 µg/mL streptomycin and 10% BSA. At 2 hrs and 16 hrs post-incubation, 70 islets per genotype were collected in 250 µL of PBS and lysed prior to DNA quantification and freezing at -20°C. A 200 µL aliquot of D31-palmitate-labelled solution was also collected and stored at -20°C. Similarly, upon overnight incubation, the remaining islets were collected in PBS, lysed and the DNA was quantified. The leftover labeling solution was also collected and frozen at -20°C for measures of background signal.

Total lipids were extracted from cell lysates (58) and prepared and analyzed by a 6890N Network GC System (Agilent Technologies; CA, USA) as previously described (59). An internal standard containing a known concentration was added to samples for the quantification of total fatty acids. Fatty acid methyl esters were identified by their retention times compared to a standard containing 31 known FAs. Intracellular D31 enrichment was determined by GC-mass spectrometry (GC-MS) using a 5890 GC coupled to a 5973N MSD (Agilent Technologies; CA, USA). Ions with mass-to-charge ratios (m/z) of M+0 and M+31 were determined by selected ion monitoring. As a marker of fatty acid oxidation, we measured the appearance of $2H_2O$ derived from D31-palmitate in cell media using a Finnigan GasBench-II (ThermoFisher Scientific, UK) (60).

Visualization of transcriptomic datasets

Details of the RNA-seq and ChIP-seq experiments, as well as human islet donors, are previously described (48, 61-63). All transcriptomic datasets used to generate Supplementary figure 1A and B are publicly available through EMBL-EBI and GEO databases, and freely-accessible through www.isletregulome.com. For visualization, processed RNA-sequencing and ChIP-seq (bigwig) data files were downloaded (EBI: E-MTAB-1919, E-MTAB-1294 and

GEO:GSE151405) and loaded onto the local open source University of California Santa Cruz (UCSC) Genome Browser (http://genome.ucsc.edu/) (64), under a private session.

Statistics

Measurements were performed on discrete samples unless otherwise stated. Data normality was assessed using D'Agostino-Person test. All analyses were conducted using GraphPad Prism software. Pairwise comparisons were made using Student's two-tailed unpaired or paired t-test. Multiple interactions were determined using one-way ANOVA or two-way ANOVA, adjusted for repeated measures where relevant. Pairwise post-hoc testing was performed using Sidak's test, or Tukey's test where more than two groups were considered. Where a highly significant interaction was detected using two-way ANOVA, but post-hoc testing was just above $P = 0.05$, multiple comparisons were accounted for using the false discovery rate followed by the two-stage linear step-up method of Benjamini, Krieger and Yekutieli. For non-parametric multiple comparison, Kruskal-Wallis test was used followed by Dunn's post hoc test. Degrees of freedom were accounted for during all post-hoc testing. A P value less than 0.05 was considered significant.

Data availability

The datasets generated and/or analyzed during the current study are available from the corresponding author upon reasonable request.

Study approval

Animal studies were regulated by the Animals (Scientific Procedures) Act 1986 of the U.K. (Personal Project License P2ABC3A83), and approval was granted by the University of Birmingham's Animal Welfare and Ethical Review Body.

AUTHOR CONTRIBUTIONS

D.N., F.C., K.V., R.B.B., R.W., J.P.B., M.H., J.W.J., J.C. and D.J.H. performed experiments and analyzed data. F.C., A.T., E.J., G.G.L., L.H. and D.T. ran and analyzed samples for GC-MS. I.A. analyzed genomic data. D.J.H and D.T. conceived and designed the studies. D.J.H. supervised the studies. D.J.H., D.N., F.C. and D.T. wrote the paper with input from all authors.

ACKNOWLEDGEMENTS

D.J.H. was supported by MRC (MR/N00275X/1 and MR/S025618/1) and Diabetes UK (17/0005681) Project Grants. D.T. was supported by Cancer Research UK Grants (C42109/A26982 and C42109/A24891). J.J. was supported by the Canadian Institute of Health Research (CIHR, PJT-159552). L.H. was supported by a British Heart Foundation Senior Fellowship (FS/15/56/31645). G.G.L. was supported by a Wellcome Trust Senior Research Fellowship (104612/Z/14/Z). This project has received funding from the European Research Council (ERC) under the European Union's Horizon 2020 research and innovation programme (Starting Grant 715884 to D.J.H.). We thank Dr Mathew Coleman (University of Birmingham) for useful discussions.

REFERENCES

1. Bruick RK. Oxygen sensing in the hypoxic response pathway: regulation of the hypoxia-inducible transcription factor. *Genes Dev.* 2003;17(21):2614-23.
2. Schofield CJ, and Ratcliffe PJ. Oxygen sensing by HIF hydroxylases. *Nat Rev Mol Cell Biol.* 2004;5(5):343-54.
3. Bruick RK, and McKnight SL. A conserved family of prolyl-4-hydroxylases that modify HIF. *Science.* 2001;294(5545):1337-40.
4. Epstein AC, Gleadle JM, McNeill LA, Hewitson KS, O'Rourke J, Mole DR, et al. C. elegans EGL-9 and mammalian homologs define a family of dioxygenases that regulate HIF by prolyl hydroxylation. *Cell.* 2001;107(1):43-54.
5. Kaelin WG, Jr., and Ratcliffe PJ. Oxygen sensing by metazoans: the central role of the HIF hydroxylase pathway. *Mol Cell.* 2008;30(4):393-402.
6. Chan DA, Kawahara TL, Sutphin PD, Chang HY, Chi JT, and Giaccia AJ. Tumor vasculature is regulated by PHD2-mediated angiogenesis and bone marrow-derived cell recruitment. *Cancer Cell.* 2009;15(6):527-38.
7. Duran RV, MacKenzie ED, Boulahbel H, Frezza C, Heiserich L, Tardito S, et al. HIF-independent role of prolyl hydroxylases in the cellular response to amino acids. *Oncogene.* 2013;32(38):4549-56.
8. Luo W, Hu H, Chang R, Zhong J, Knabel M, O'Meally R, et al. Pyruvate kinase M2 is a PHD3-stimulated coactivator for hypoxia-inducible factor 1. *Cell.* 2011;145(5):732-44.
9. Henze AT, Garvalov BK, Seidel S, Cuesta AM, Ritter M, Filatova A, et al. Loss of PHD3 allows tumours to overcome hypoxic growth inhibition and sustain proliferation through EGFR. *Nat Commun.* 2014;5:5582.
10. Appelhoff RJ, Tian Y-M, Raval RR, Turley H, Harris AL, Pugh CW, et al. Differential Function of the Prolyl Hydroxylases PHD1, PHD2, and PHD3 in the Regulation of Hypoxia-inducible Factor. *Journal of Biological Chemistry.* 2004;279(37):38458-65.

11. Berra E, Benizri E, Ginouves A, Volmat V, Roux D, and Pouyssegur J. HIF prolyl-hydroxylase 2 is the key oxygen sensor setting low steady-state levels of HIF-1alpha in normoxia. *EMBO J.* 2003;22(16):4082-90.
12. Tennant DA, Frezza C, MacKenzie ED, Nguyen QD, Zheng L, Selak MA, et al. Reactivating HIF prolyl hydroxylases under hypoxia results in metabolic catastrophe and cell death. *Oncogene.* 2009;28(45):4009-21.
13. Kiss J, Mollenhauer M, Walmsley SR, Kirchberg J, Radhakrishnan P, Niemietz T, et al. Loss of the oxygen sensor PHD3 enhances the innate immune response to abdominal sepsis. *J Immunol.* 2012;189(4):1955-65.
14. Walmsley SR, Chilvers ER, Thompson AA, Vaughan K, Marriott HM, Parker LC, et al. Prolyl hydroxylase 3 (PHD3) is essential for hypoxic regulation of neutrophilic inflammation in humans and mice. *Journal of Clinical Investigation.* 2011;121(3):1053-63.
15. Su Y, Loos M, Giese N, Hines OJ, Diebold I, Gorlach A, et al. PHD3 regulates differentiation, tumour growth and angiogenesis in pancreatic cancer. *Br J Cancer.* 2010;103(10):1571-9.
16. Schlisio S, Kenchappa RS, Vredeveld LC, George RE, Stewart R, Greulich H, et al. The kinesin KIF1Bbeta acts downstream from EglN3 to induce apoptosis and is a potential 1p36 tumor suppressor. *Genes Dev.* 2008;22(7):884-93.
17. Place TL, and Domann FE. Prolyl-hydroxylase 3: Evolving Roles for an Ancient Signaling Protein. *Hypoxia (Auckl).* 2013;2013(1):13-7.
18. Tennant DA, and Gottlieb E. HIF prolyl hydroxylase-3 mediates alpha-ketoglutarate-induced apoptosis and tumor suppression. *Journal of Molecular Medicine.* 2010;88(8):839-49.
19. Boulahbel H, Durán Raúl V, and Gottlieb E. Prolyl hydroxylases as regulators of cell metabolism. *Biochemical Society Transactions.* 2009;37(1):291-4.

686 20. Chen N, Rinner O, Czernik D, Nytko KJ, Zheng D, Stiehl DP, et al. The oxygen
687 sensor PHD3 limits glycolysis under hypoxia via direct binding to pyruvate kinase.
688 *Cell Research.* 2011;21(6):983-6.
689 21. Lee S, Nakamura E, Yang H, Wei W, Linggi MS, Sajan MP, et al. Neuronal apoptosis
690 linked to EglN3 prolyl hydroxylase and familial pheochromocytoma genes:
691 Developmental culling and cancer. *Cancer Cell.* 2005;8(2):155-67.
692 22. Dang L, White DW, Gross S, Bennett BD, Bittinger MA, Driggers EM, et al. Cancer-
693 associated IDH1 mutations produce 2-hydroxyglutarate. *Nature.*
694 2009;462(7274):739-44.
695 23. Tomlinson IP, Alam NA, Rowan AJ, Barclay E, Jaeger EE, Kelsell D, et al. Germline
696 mutations in FH predispose to dominantly inherited uterine fibroids, skin leiomyomata
697 and papillary renal cell cancer. *Nat Genet.* 2002;30(4):406-10.
698 24. German NJ, Yoon H, Yusuf RZ, Murphy JP, Finley LW, Laurent G, et al. PHD3 Loss
699 in Cancer Enables Metabolic Reliance on Fatty Acid Oxidation via Deactivation of
700 ACC2. *Mol Cell.* 2016;63(6):1006-20.
701 25. Taniguchi CM, Finger EC, Krieg AJ, Wu C, Diep AN, LaGory EL, et al. Cross-talk
702 between hypoxia and insulin signaling through Phd3 regulates hepatic glucose and
703 lipid metabolism and ameliorates diabetes. *Nature Medicine.* 2013;19(10):1325-30.
704 26. Yano H, Sakai M, Matsukawa T, Yagi T, Naganuma T, Mitsushima M, et al. PHD3
705 regulates glucose metabolism by suppressing stress-induced signalling and
706 optimising gluconeogenesis and insulin signalling in hepatocytes. *Sci Rep.*
707 2018;8(1):14290.
708 27. Huang M, Paglialunga S, Wong JMK, Hoang M, Pillai R, and Joseph JW. Role of
709 prolyl hydroxylase domain proteins in the regulation of insulin secretion. *Physiological*
710 *Reports.* 2016;4(5):e12722.
711 28. De Vos A, Heimberg H, Quartier E, Huypens P, Bouwens L, Pipeleers D, et al.
712 Human and rat beta cells differ in glucose transporter but not in glucokinase gene
713 expression. *Journal of Clinical Investigation.* 1995;96(5):2489-95.

29. German MS. Glucose sensing in pancreatic islet beta cells: the key role of glucokinase and the glycolytic intermediates. *Proceedings of the National Academy of Sciences of the United States of America.* 1993;90(5):1781-5.
30. Rutter GA, Pullen TJ, Hodson DJ, and Martinez-Sanchez A. Pancreatic beta-cell identity, glucose sensing and the control of insulin secretion. *Biochemical Journal.* 2015;466(2):203-18.
31. Pullen TJ, and Rutter GA. When less is more: the forbidden fruits of gene repression in the adult beta-cell. *Diabetes Obes Metab.* 2013;15(6):503-12.
32. Lemaire K, Thorrez L, and Schuit F. Disallowed and Allowed Gene Expression: Two Faces of Mature Islet Beta Cells. *Annu Rev Nutr.* 2016;36:45-71.
33. Thorens B, Tarussio D, Maestro MA, Rovira M, Heikkila E, and Ferrer J. Ins1(Cre) knock-in mice for beta cell-specific gene recombination. *Diabetologia.* 2015;58(3):558-65.
34. Takeda K, Ho VC, Takeda H, Duan L-J, Nagy A, and Fong G-H. Placental but Not Heart Defects Are Associated with Elevated Hypoxia-Inducible Factor α Levels in Mice Lacking Prolyl Hydroxylase Domain Protein 2. *Molecular and Cellular Biology.* 2006;26(22):8336-46.
35. Mosleh E, Ou K, Haemmerle MW, Tembo T, Yuhas A, Carboneau BA, et al. Ins1-Cre and Ins1-CreER Gene Replacement Alleles Are Susceptible To Silencing By DNA Hypermethylation. *Endocrinology.* 2020;161(8).
36. Johnston Natalie R, Mitchell Ryan K, Haythorne E, Pessoa Maria P, Semplici F, Ferrer J, et al. Beta Cell Hubs Dictate Pancreatic Islet Responses to Glucose. *Cell Metabolism.* 2016;24(3):389-401.
37. Nasteska D, Fine NHF, Ashford FB, Cuozzo F, Viloria K, Smith G, et al. PDX1(LOW) MAFA(LOW) beta-cells contribute to islet function and insulin release. *Nat Commun.* 2021;12(1):674.

38. Blodgett DM, Nowosielska A, Afik S, Pechhold S, Cura AJ, Kennedy NJ, et al. Novel Observations From Next-Generation RNA Sequencing of Highly Purified Human Adult and Fetal Islet Cell Subsets. *Diabetes.* 2015;64(9):3172-81.
39. Benner C, van der Meulen T, Caceres E, Tigyi K, Donaldson CJ, and Huising MO. The transcriptional landscape of mouse beta cells compared to human beta cells reveals notable species differences in long non-coding RNA and protein-coding gene expression. *BMC Genomics.* 2014;15:620.
40. Komatsu H, Cook C, Wang CH, Medrano L, Lin H, Kandeel F, et al. Oxygen environment and islet size are the primary limiting factors of isolated pancreatic islet survival. *PLoS One.* 2017;12(8):e0183780.
41. Nauck MA, Homberger E, Siegel EG, Allen RC, Eaton RP, Ebert R, et al. Incretin effects of increasing glucose loads in man calculated from venous insulin and C-peptide responses. *Journal of Clinical Endocrinology and Metabolism.* 1986;63(2):492-8.
42. da Silva Xavier G, and Hodson DJ. Mouse models of peripheral metabolic disease. *Best Pract Res Clin Endocrinol Metab.* 2018;32(3):299-315.
43. Cantley J, Davenport A, Vetterli L, Nemes NJ, Whitworth PT, Boslem E, et al. Disruption of beta cell acetyl-CoA carboxylase-1 in mice impairs insulin secretion and beta cell mass. *Diabetologia.* 2019;62(1):99-111.
44. Yoon H, Spinelli JB, Zaganjor E, Wong SJ, German NJ, Randall EC, et al. PHD3 Loss Promotes Exercise Capacity and Fat Oxidation in Skeletal Muscle. *Cell Metab.* 2020;32(2):215-28 e7.
45. Ronnebaum SM, Joseph JW, Ilkayeva O, Burgess SC, Lu D, Becker TC, et al. Chronic Suppression of Acetyl-CoA Carboxylase 1 in β-Cells Impairs Insulin Secretion via Inhibition of Glucose Rather Than Lipid Metabolism. *Journal of Biological Chemistry.* 2008;283(21):14248-56.

766 46. MacDonald MJ, Dobrzyn A, Ntambi J, and Stoker SW. The role of rapid lipogenesis
767 in insulin secretion: Insulin secretagogues acutely alter lipid composition of INS-1
768 832/13 cells. *Archives of Biochemistry and Biophysics.* 2008;470(2):153-62.
769 47. Hrvatin S, O'Donnell CW, Deng F, Millman JR, Pagliuca FW, DiIorio P, et al.
770 Differentiated human stem cells resemble fetal, not adult, β cells. *Proceedings of the*
771 *National Academy of Sciences.* 2014;111(8):3038-43.
772 48. Moran I, Akerman I, van de Bunt M, Xie R, Benazra M, Nammo T, et al. Human beta
773 Cell Transcriptome Analysis Uncovers lncRNAs That Are Tissue-Specific,
774 Dynamically Regulated, and Abnormally Expressed in Type 2 Diabetes. *Cell*
775 *Metabolism.* 2012;16(4):435-48.
776 49. Cantley J, Selman C, Shukla D, Abramov AY, Forstreuter F, Esteban MA, et al.
777 Deletion of the von Hippel-Lindau gene in pancreatic beta cells impairs glucose
778 homeostasis in mice. *J Clin Invest.* 2009;119(1):125-35.
779 50. Cockman ME, Lippl K, Tian YM, Pegg HB, Figg WDJ, Abboud MI, et al. Lack of
780 activity of recombinant HIF prolyl hydroxylases (PHDs) on reported non-HIF
781 substrates. *Elife.* 2019;8:e46490.
782 51. Taniguchi CM, Finger EC, Krieg AJ, Wu C, Diep AN, LaGory EL, et al. Cross-talk
783 between hypoxia and insulin signaling through Phd3 regulates hepatic glucose and
784 lipid metabolism and ameliorates diabetes. *Nat Med.* 2013;19(10):1325-30.
785 52. Bishop T, Gallagher D, Pascual A, Lygate CA, de Bono JP, Nicholls LG, et al.
786 Abnormal sympathoadrenal development and systemic hypotension in PHD3-/- mice.
787 *Mol Cell Biol.* 2008;28(10):3386-400.
788 53. Cantley J, Walters SN, Jung M-H, Weinberg A, Cowley MJ, Whitworth PT, et al. A
789 Preexistent Hypoxic Gene Signature Predicts Impaired Islet Graft Function and
790 Glucose Homeostasis. *Cell Transplantation.* 2013;22(11):2147-59.
791 54. Hodson DJ, Mitchell RK, Marselli L, Pullen TJ, Gimeno Brias S, Semplici F, et al.
792 ADCY5 couples glucose to insulin secretion in human islets. *Diabetes.*
793 2014;63(9):3009-21.

55. Berg J, Hung YP, and Yellen G. A genetically encoded fluorescent reporter of ATP:ADP ratio. *Nat Methods.* 2009;6(2):161-6.
56. Wortham M, Benthuysen JR, Wallace M, Savas JN, Mulas F, Divakaruni AS, et al. Integrated In Vivo Quantitative Proteomics and Nutrient Tracing Reveals Age-Related Metabolic Rewiring of Pancreatic beta Cell Function. *Cell Rep.* 2018;25(10):2904-18 e8.
57. Hiller K, Hangebrauk J, Jäger C, Spura J, Schreiber K, and Schomburg D. MetaboliteDetector: Comprehensive Analysis Tool for Targeted and Nontargeted GC/MS Based Metabolome Analysis. *Analytical Chemistry.* 2009;81(9):3429-39.
58. Folch J, Lees M, and Sloane Stanley GH. A simple method for the isolation and purification of total lipides from animal tissues. *J Biol Chem.* 1957;226(1):497-509.
59. Gunn PJ, Green CJ, Pramfalk C, and Hodson L. In vitro cellular models of human hepatic fatty acid metabolism: differences between Huh7 and HepG2 cell lines in human and fetal bovine culturing serum. *Physiol Rep.* 2017;5(24):e13532.
60. Law LK, Tang NL, Hui J, Ho CS, Ruiter J, Fok TF, et al. A novel functional assay for simultaneous determination of total fatty acid beta-oxidation flux and acylcarnitine profiling in human skin fibroblasts using (2)H(31)-palmitate by isotope ratio mass spectrometry and electrospray tandem mass spectrometry. *Clin Chim Acta.* 2007;382(1-2):25-30.
61. Akerman I, Tu Z, Beucher A, Rolando DMY, Sauty-Colace C, Benazra M, et al. Human Pancreatic beta Cell lncRNAs Control Cell-Specific Regulatory Networks. *Cell Metab.* 2017;25(2):400-11.
62. Pasquali L, Gaulton KJ, Rodríguez-Seguí SA, Mularoni L, Miguel-Escalada I, Akerman İ, et al. Pancreatic islet enhancer clusters enriched in type 2 diabetes risk-associated variants. *Nature Genetics.* 2014;46(2):136-43.
63. Akerman I, Maestro MA, De Franco E, Grau V, Flanagan S, Garcia-Hurtado J, et al. Neonatal diabetes mutations disrupt a chromatin pioneering function that activates the human insulin gene. *Cell Rep.* 2021;35(2):108981.

64. Kent WJ, Sugnet CW, Furey TS, Roskin KM, Pringle TH, Zahler AM, et al. The Human Genome Browser at UCSC. *Genome Research.* 2002;12(6):996-1006.

FIGURES AND LEGENDS

FIGURE 1

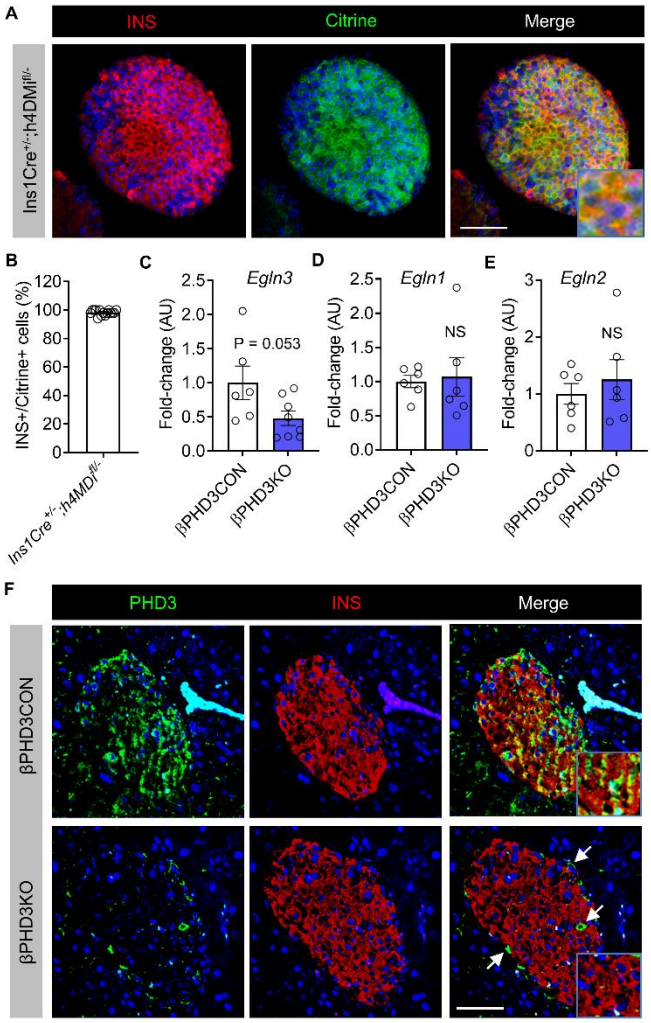

Figure 1: **Generation and validation of mice lacking PHD3 in pancreatic β-cells.** (A) Confirmation of recombination efficiency in *Ins1Cre* islets using *R26-LSL-hM4Di/mCitrine* mice expressing an mCitrine reporter (representative image shown, scale bar = 42.5 µm). (B) Percentage of insulin–positive (INS+) cells expressing mCitrine (i.e. recombined) in Ins1Cre$^{+/-}$;h4MDi$^{fl/-}$ islets (n = 15 islets). (C) *Egln3* expression is reduced in islets of βPHD3KO mice versus control (βPHD3CON) littermates (n = 6-8 animals, unpaired t-test). (D and E) *Egln1* (D) *and Egln2* (E*)* expression levels are similar in βPHD3CON and βPHD3KO islets (n = 6 animals, unpaired t-test). (F) PHD3 is detected in the β-cell compartment of βPHD3CON but not βPHD3KO islets. Arrows show PHD3 expression in non β-cells (representative images shown, scale bar = 42.5 µm) (n = 3 animals/genotype). Data shown are mean ± SEM. *P<0.05, **P<0.01 and NS, non-significant. *Egln1/Egln2/Egln3,* Eglnine homolog 1-3 genes; PHD3, prolyl-hydroxylase 3.

FIGURE 2

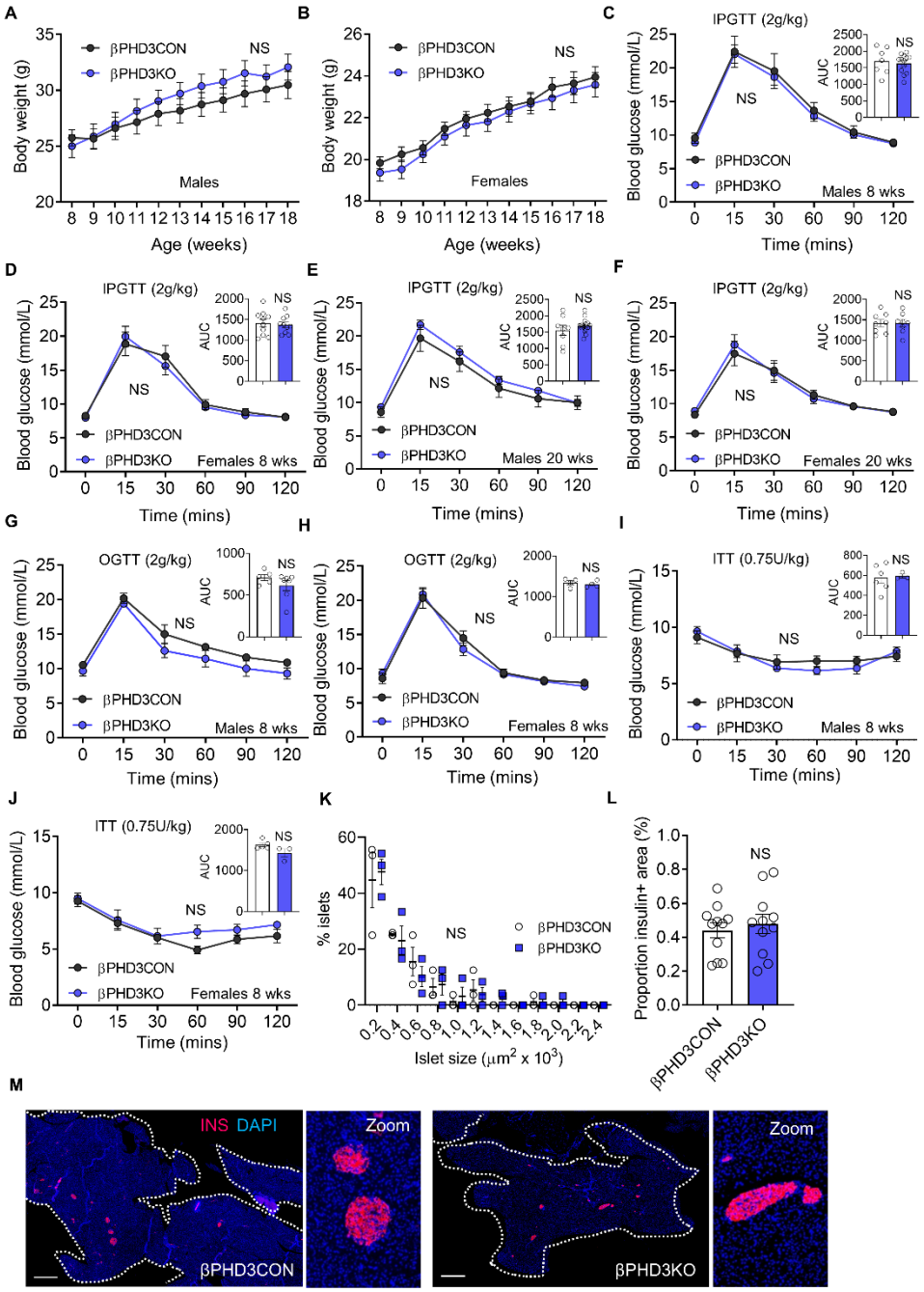

839

840 **Figure 2**: **βPHD3KO *in vivo* phenotype under standard chow conditions.** (A and B) Male
841 (A) and female (B) βPHD3CON and βPHD3KO mice possess similar adult body weight (n =
842 8-10 male and 15 female animals/genotype, two-way RM ANOVA; Sidak's test). (C and D) No
843 differences in glucose tolerance and AUC are detected between βPHD3CON and βPHD3KO
844 male (C) (n = 13 animals/genotype) and female (D) (n = 10 animals/genotype) 8-week-old
845 mice (two-way RM ANOVA, Sidak's test) (AUC: unpaired t-test). (E and F) No differences in
846 glucose tolerance and AUC during IPGTT are detected between βPHD3CON and βPHD3KO
847 male (E) and female (F) 20-week-old mice (n = 8-16 male and 8 female animals/genotype;
848 two-way RM ANOVA, Sidak's test) (AUC: unpaired t-test). (G and H) Oral glucose tolerance
849 and AUC are also unchanged in βPHD3KO versus βPHD3CON male (G) and female (H) 8-
850 week-old mice (n = 3-5 male and 4 female animals/genotype; two-way RM ANOVA, Sidak's

test) (AUC: unpaired t-test). (I and J) Insulin sensitivity and AUC are similar in βPHD3CON and βPHD3KO male (I) and female (J) 8-week old mice (n = 6-7 male and 4-7 female animals/genotype; two-way RM ANOVA, Sidak's test) (AUC: unpaired t-test). (K-M) Cell resolution reconstruction of entire pancreatic sections shows no differences in islet size and β-cell mass between βPHD3CON and βPHD3KO mice. Quantification is shown in (K and L), with representative images in (M) (scale bar = 530 μm) (zoom showing maintenance of cellular resolution in a single image) (K; n = 3 animals/genotype, two-way ANOVA; Sidak's test) (L; n = 3 animals/genotype, unpaired t-test). Data shown are mean ± SEM. *P<0.05, **P<0.01 and NS, non-significant. IPGTT, intraperitoneal glucose tolerance test; OGTT, oral glucose tolerance test; AUC, area under the curve.

FIGURE 3

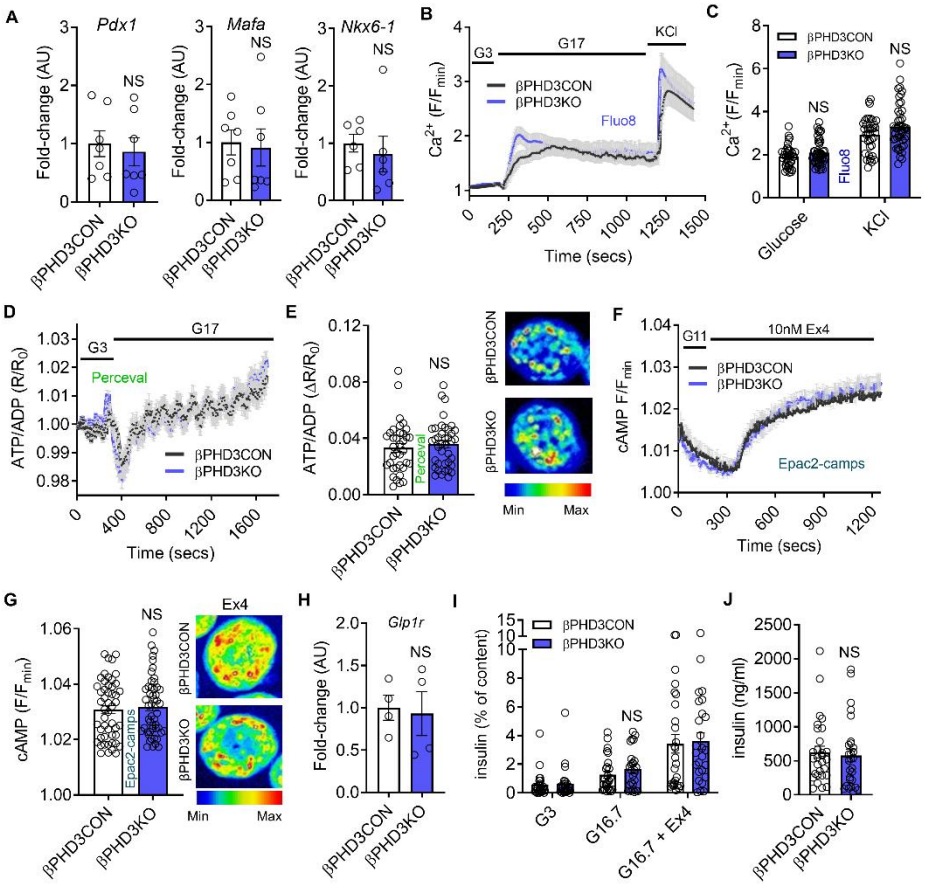

Figure 3: **βPHD3KO *in vitro* phenotype under standard chow conditions.** (A) Expression of the β-cell-specific markers *Pdx1*, *Mafa* and *Nkx6.1* is similar in βPHD3CON and βPHD3KO islets (n = 6-7 animals, unpaired t-test). (B and C) Glucose- and KCl-stimulated Ca^{2+} rises do not differ in islets of βPHD3CON and βPHD3KO mice, shown by mean traces (B), and summary bar graph (C) (n = 38-48 islets, 4-5 animals/genotype; two-way ANOVA, Sidak's test). (D and E) Glucose-stimulated ATP/ADP rises are similar in βPHD3CON and βPHD3KO islets, shown by mean traces (D) and summary bar graph (E) (representative images shown; a single islet has been cropped for clarity) (n = 36-39 islets, 4-5 animals/genotype, unpaired t-test). (F and G) cAMP responses to Ex4 do not differ between βPHD3CON and βPHD3KO islets, shown by (F) mean traces and (G) summary bar graph (representative images shown; a single islet has been cropped for clarity) (n = 50 islets, 4-5 animals/genotype, unpaired t-test). (H) *Glp1r* expression is similar in βPHD3CON and βPHD3KO islets (n = 4 animals/genotype, unpaired t-test). (I) Insulin secretory responses to glucose and Exendin-4 show no differences between βPHD3CON and βPHD3KO islets (n = 29 replicates, 6 animals/genotype, two-way ANOVA; Sidak's test). (J) Total insulin content also remained similar between groups (n = 29 replicates, 6 animals/genotype; unpaired t-test). Data shown are mean± SEM. *P<0.05, **P<0.01 and NS, non-significant. G3, 3 mM glucose; G16.7, 16.7 mM glucose; G17, 17 mM glucose.

FIGURE 4

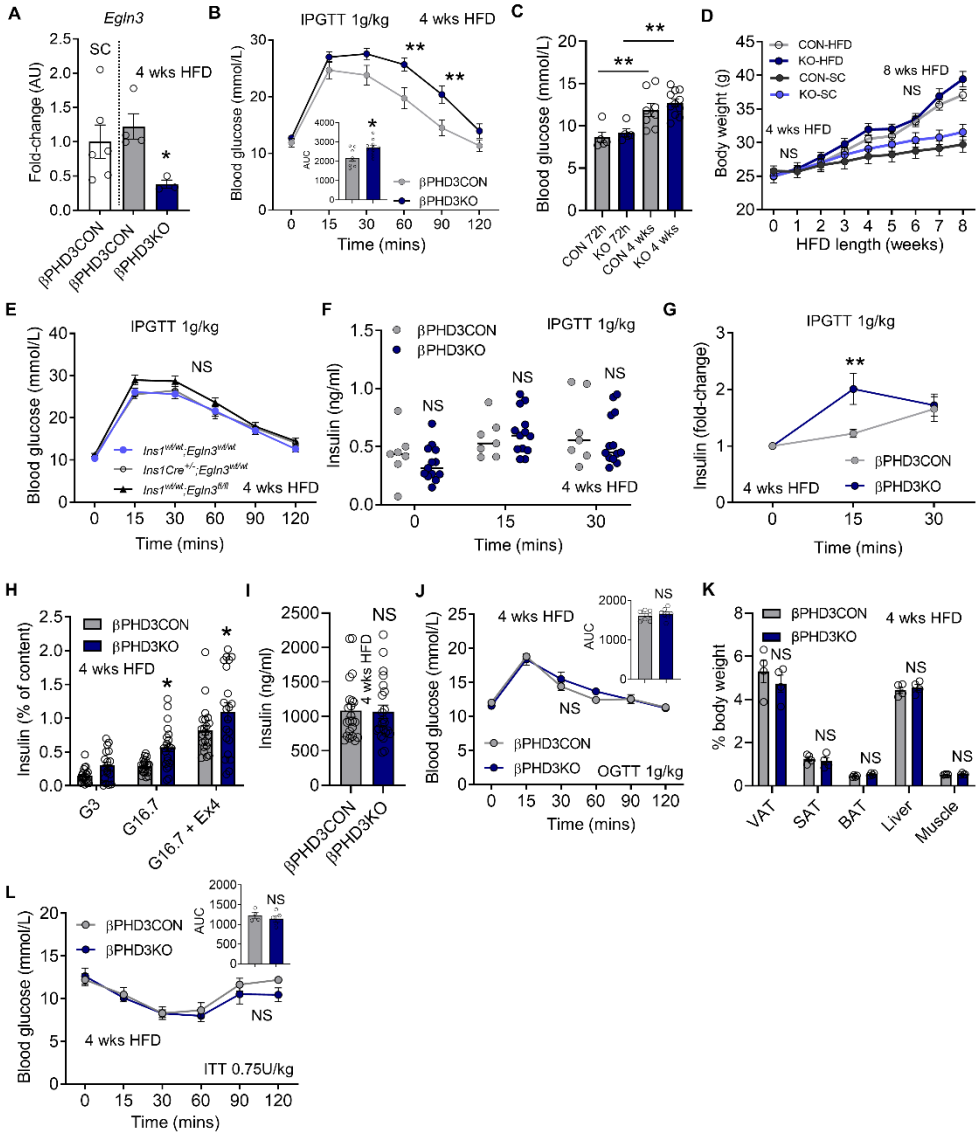

Figure 4: **βPHD3KO *in vivo* and *in vitro* phenotype during early metabolic stress (4 weeks HFD).** (A) *Egln3* is upregulated in 4 weeks HFD βPHD3CON, but not βPHD3KO islets (n = 3-6 animals/genotype; unpaired t-test). (B and C) Glucose tolerance (B) is impaired in male βPHD3KO mice at 4 weeks HFD, although fasting glucose levels (C) are unaffected by 72 hrs HFD (n = 8-11 animals/genotype; two-way RM ANOVA, Sidak's test). (D) Body weight is similar in male HFD-fed βPHD3CON and βPHD3KO animals (n = 11-12 animals/genotype; two-way RM ANOVA. Sidak's test). Body weight data from Figure 2A is included for comparison. (E) Glucose tolerance is unaffected in male *Cre*-only and *Egln3*$^{fl/fl}$-only controls (n = 10-13 animals/genotype; two-way RM ANOVA, Tukey's test). (F) Serum insulin levels post-glucose are similar in βPHD3CON and βPHD3KO mice (n = 7-13 mice/genotype; two-way RM ANOVA, Sidak's test). (G) Insulin responses to glucose, shown by stimulation index, are higher in male βPHD3KO mice (n = 7-13 animals/genotype; two-way RM ANOVA, Sidak's test). (H and I) Glucose- and Exendin-4-potentiated insulin secretion is increased in βPHD3KO islets(H) (n = 20 replicates, 4 animals/genotype; two-way ANOVA, Sidak's test), while insulin content (I) remains unchanged (n = 20 replicates, 4 mice/genotype; unpaired t-test). (J) βPHD3CON and βPHD3KO mice show similar oral glucose tolerance (n = 7 animals/genotype; two-way RM ANOVA, Sidak's test). (K) No changes in body compostion are seen in βPHD3KO vs βPHD3CON mice (n = 4 animals/genotype; two-way ANOVA, Sidak's test). (L) Insulin sensitivity remains unchanged in βPHD3KO mice (n = 4-5

910 animals/genotype; two-way RM ANOVA, Sidak's test). Data shown are mean ± SEM. *P<0.05,
911 **P<0.01 and NS, non-significant. VAT/SAT/BAT, visceral/subcutaneous/brown adipose
912 tissue.

913

914

FIGURE 5

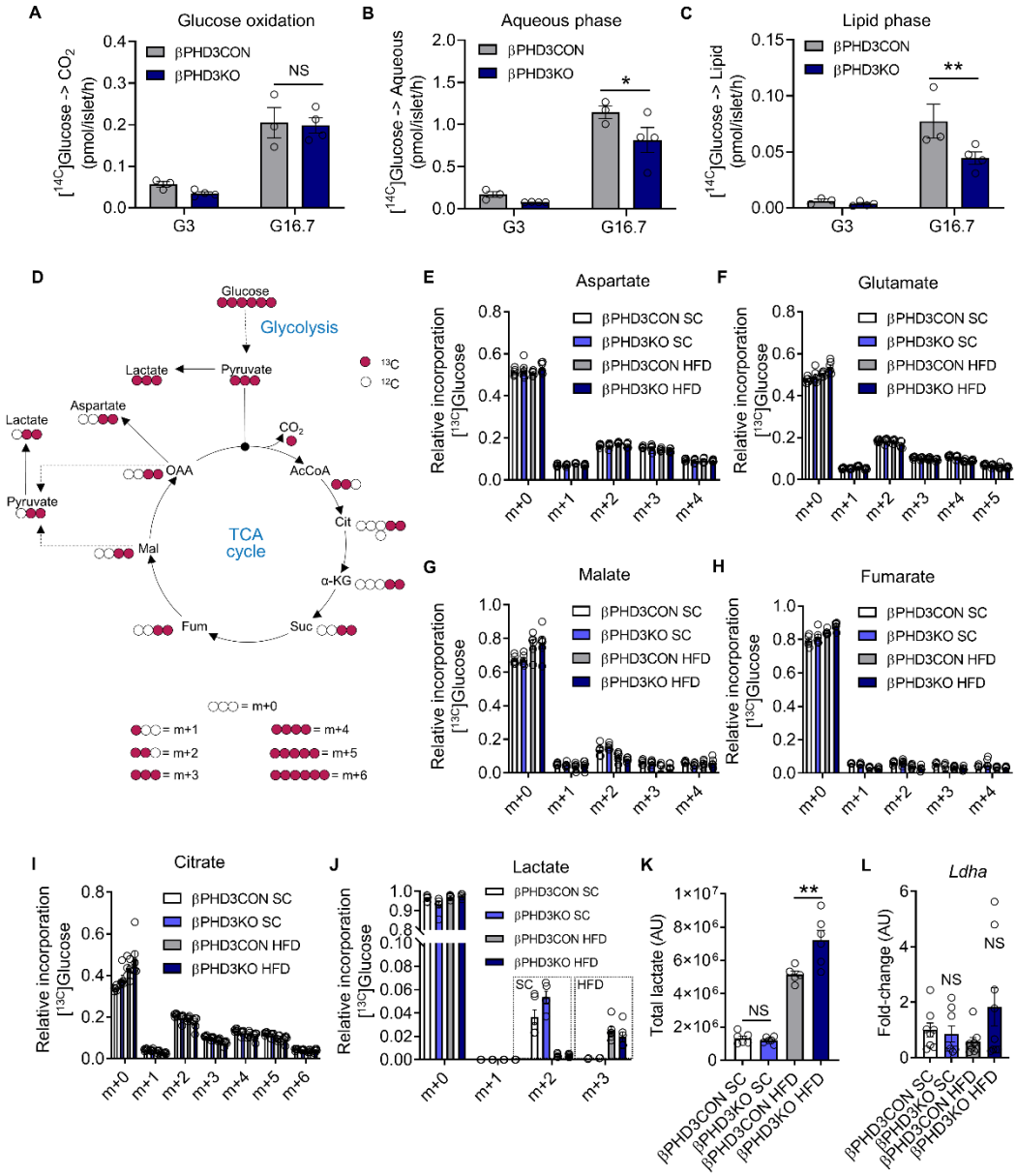

Figure 5: **Metabolic rewiring in βPHD3KO islets during metabolic stress.** (A-C) βPHD3KO islets possess intact glucose oxidation (A), but impaired accumulation of glycolytic/TCA cycle metabolites (B) and glucose-driven lipogenesis (C) following 4 weeks of HFD (n = 3 islet preparations, 3 animals/genotype; two-way ANOVA, Benjamini- Krieger-Yekutieli two-stage procedure). (D) Schematic showing ^{13}C from $^{13}C_6$-[U]-glucose incorporation into metabolites in βPHD3CON and βPHD3KO islets. (E-I) Mass isotopomer distributions (MID) showing that ^{13}C incorporation from glucose into aspartate (E), glutamate (F), malate (G), fumarate (H) or citrate (I) is similar in SC and HFD βPHD3CON and βPHD3KO islets (n = 6 islet preparations, 3 animals/genotype, two-way ANOVA, Tukey's test). (J) ^{13}C from $^{13}C_6$-[U]-glucose is incorporated primarily into m+2 lactate in SC βPHD3CON and βPHD3KO islets, whereas a shift to m+3 lactate is seen during 4 weeks HFD (n = 6 islet preparations, 3 animals/genotype; two-way ANOVA, Tukey's test). (K) Steady-state lactate levels are increased in βPHD3KO versus βPHD3CON islets following 4 weeks HFD (n = 6 islet preparations, n = 3 animals/genotype; one-way ANOVA, Sidak's test). (L) *Ldha* expression is not significantly

different in SC and HFD βPHD3KO and βPHD3CON islets (n = 8-9 animals/genotype; Dunnett's test). Data shown are mean ± SEM. *P<0.05, **P<0.01 and NS, non-significant.

FIGURE 6

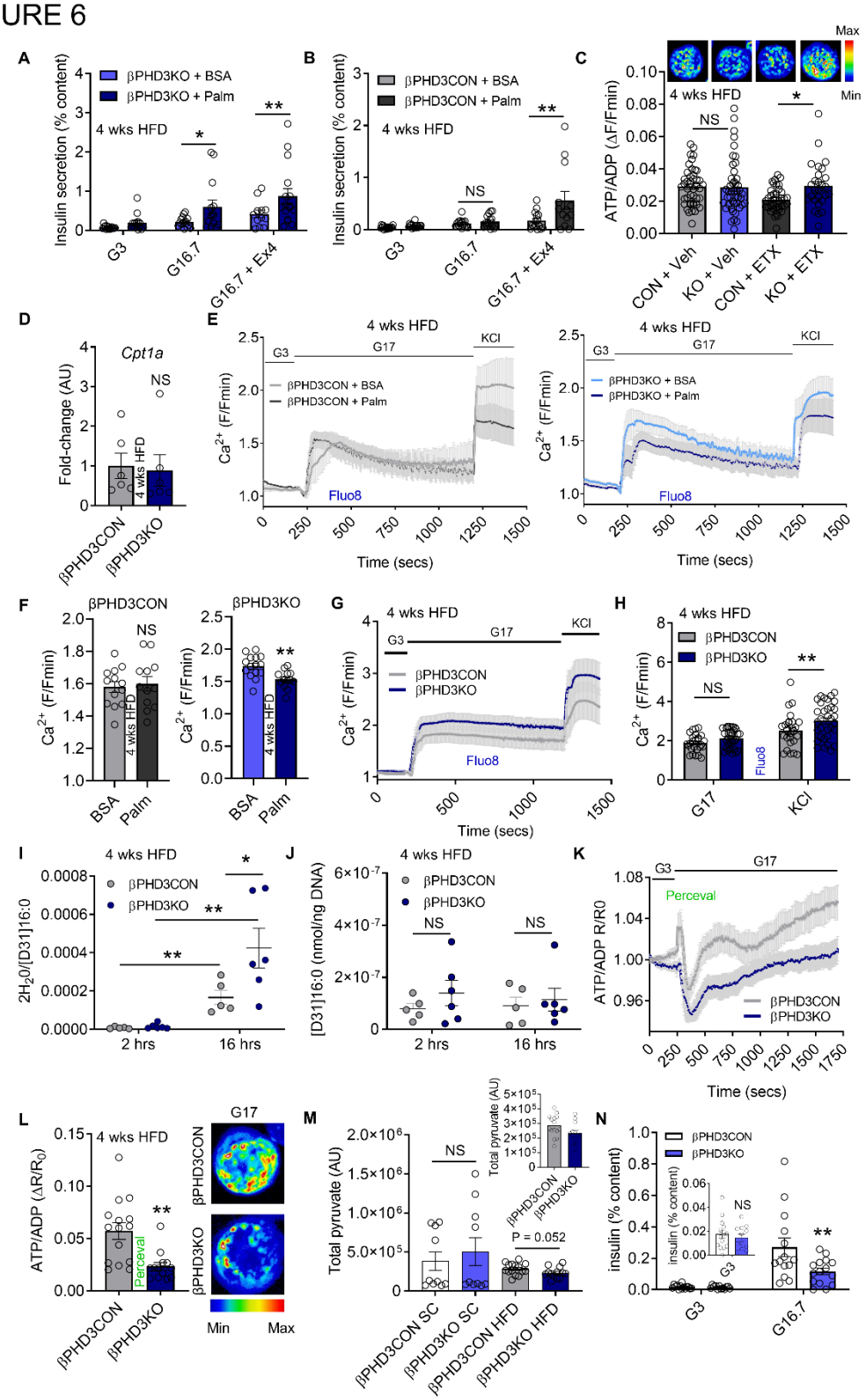

Figure 6: Nutrient preference is altered in βPHD3KO islets during early metabolic stress (4 weeks HFD). (A) Palmitate (Palm) enhances glucose- and Exendin-4-stimulated insulin secretion in βPHD3KO islets (n = 12-17 replicates, 7-9 animals/genotype; two-way ANOVA, Benjamini- Krieger-Yekutieli two-stage procedure) (BSA, bovine serum albumin). (B) As for (A), but showing glucose and Exendin-4 response in βPHD3CON islets (n = 13-17 replicates, 7-9 animals/genotype; two-way, ANOVA, Benjamini- Krieger-Yekutieli two-stage procedure).

(C) Etomoxir (ETX) increases glucose-stimulated ATP/ADP ratio in βPHD3KO islets (representative images show a single islet) (n = 27-45 islets, 5-6 animals/genotype; two-way ANOVA, Sidak's test). (D) *Cpt1a* expression is similar in βPHD3KO and βPHD3CON islets (n = 6 animals/genotype; unpaired t-test). (E and F) Palmitate impairs Ca^{2+} responses to glucose in βPHD3KO islets, shown by mean traces (E) and bar graphs (F) (n = 13-15 islets, 2-3 animals/genotype, unpaired t-test). (G and H) Glucose- and KCl-stimulated Ca^{2+} rises are similar to controls (glucose), or increased (KCl), in βPHD3KO islets, shown by mean traces (G) and a bar graph (H) (n = 26-33 islets, 6 animals/genotype; two-way ANOVA, Sidak's test). (I) $2H_20$/D31-palmitate ratio is increased in βPHD3KO islets (n = 5-6 animals) (within genotype: unpaired t-test) (between genotype: two-way ANOVA, Sidak's test). (J) D31-palmitate tracer uptake is similar in βPHD3CON and βPHD3KO islets (n = 5-6 animals; two-way ANOVA, Sidak's test). (K and L) ATP/ADP rises are impaired in βPHD3KO islets, shown by mean traces (K), bar graph and representative images (L) (single islet shown) (n = 13-15 islets, 4 animals/genotype, unpaired t-test). (M) Steady-state pyruvate levels are decreased in βPHD3KO islets (n = 11-13 replicates, 5-8 animals/genotype; Mann-Whitney test). (N) Low glucose pre-incubation decreases glucose-stimulated insulin secretion in SC βPHD3KO islets (n = 14-15 replicates, 6 animals/genotype; two-way ANOVA, Sidak's test). Data shown are mean ± SEM. *P<0.05, **P<0.01 and NS, non-significant.

FIGURE 7

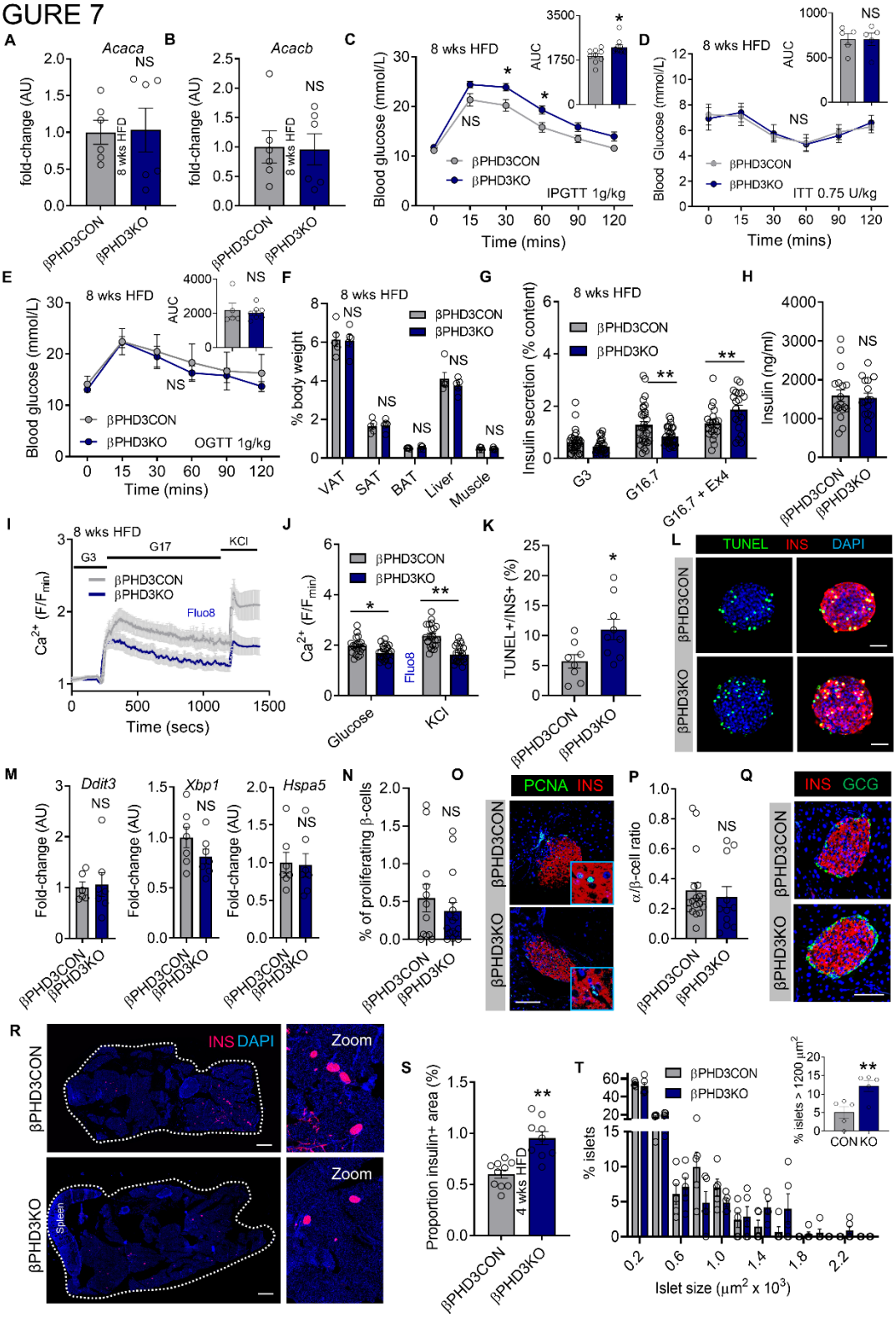

Figure 7: Prolonged metabolic stress (8 weeks HFD) leads to insulin secretory failure in βPHD3KO islets. (A and B) *Acaca* (A) and *Acacb* (B) expression is similar in βPHD3KO and βPHD3CON HFD islets (n = 6 animals; unpaired t-test). (C) Glucose tolerance remains impaired in 8 weeks HFD βPHD3KO mice (n = 9-11 animals/genotype (two-way RM ANOVA, Sidak's test) (AUC: unpaired t-test). (D) Insulin sensitivity is unchanged in βPHD3KO mice (n = 5 animals/genotype, two-way RM ANOVA; Sidak's test) (AUC: unpaired t-test). (E) Oral

glucose tolerance is normal in βPHD3KO mice (n = 6-7 animals/genotype; two-way RM ANOVA, Sidak's test) (AUC: unpaired t-test). (F) Body composition is unchanged in βPHD3KO mice (n = 5 animals/genotype; two-way ANOVA, Sidak's test). (G and H) Glucose-stimulated insulin secretion (G) is impaired in 8 weeks HFD βPHD3KO islets (n = 29-32 replicates, 4 animals/genotype; two-way ANOVA, Sidak's test), despite similar insulin content (H) (16-18 replicates, 4 mice/genotype; unpaired t-test). (I and J) Glucose- and KCl-stimulated Ca^{2+} rises are impaired in βPHD3KO islets, shown by mean traces (I) and quantification (J) (n = 21-24 islets, 2 animals/genotype; two-way ANOVA, Sidak's test). (K and L) Apoptosis is increased in βPHD3KO islets, shown by quantification (K) and representative images (L) (n = 8-9 islets; unpaired t-test). (M) *Ddit3, Xbp1* and *Hspa5* expression shows no changes in βPHD3KO islets (n = 6-7 animals/genotype; unpaired t-test). (N-Q) Islet proliferation (PCNA; N and O) and α-cell/β-cell ratio (P and Q) are unchanged in βPHD3KO islets (n = 11-18 islets, 3-4 animals/genotype; unpaired t-test). (R-T) Images (R) and quantification (S and T) showing increased β-cell mass in βPHD3KO mice (scale bar = 530 µm) (n = 3 animals/genotype, two-way ANOVA; unpaired t-test). Data shown are mean ± SEM. *P<0.05, **P<0.01 and NS, non-significant. Scale bar = 42.5 µm unless otherwise stated.

FIGURE 8

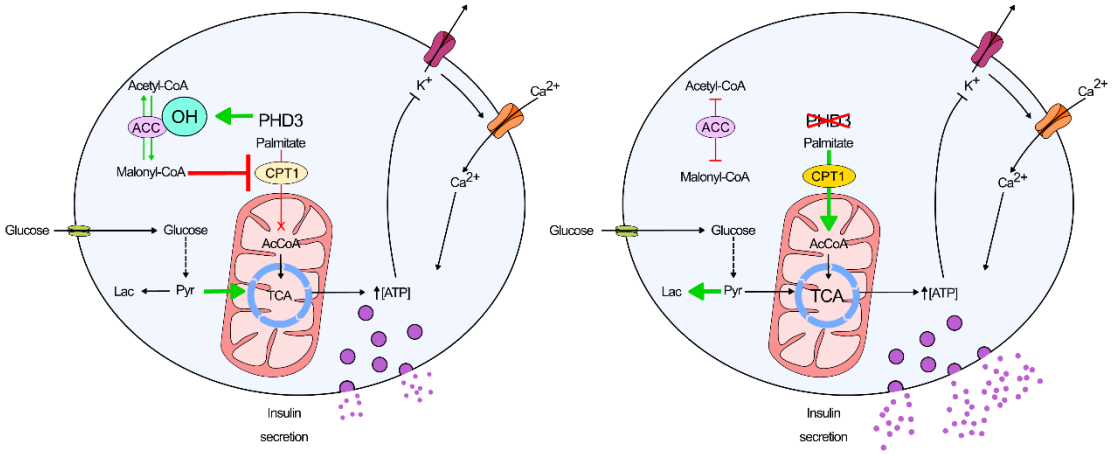

986

987 **Figure 8: Schematic showing the proposed changes that occur in PHD3KO islets**
988 **following high fat diet.** In βPHD3CON islets, glucose is converted to pyruvate, before
989 entering the TCA cycle to drive ATP production and insulin secetion. PHD3 activity leads to
990 generation of malonyl-CoA, which inhibits CPT1 to suppress oxidation of fatty acids. By
991 contrast, in βPHD3KO islets, CPT1 is no longer inhibited, allowing beta oxidation of fatty acids
992 to procede. As a result, fatty acid-derived acetyl-CoA feeds the TCA cycle and generates
993 ATP/ADP, whilst glycolytically-derived pyruvate is converted to lactate to maintain REDOX
994 status.